© 2022. Published by The Company of Biologists Ltd | Development (2022) 149, dev200110. doi:10.1242/dev.200110

RESEARCH ARTICLE

Mechanisms underlying the cooperation between loss of epithelial polarity and Notch signaling during neoplastic growth in *Drosophila*

Rémi Logeay[1], Charles Géminard[1], Patrice Lassus[2], Miriam Rodríguez-Vázquez[1], Diala Kantar[1], Lisa Heron-Milhavet[1], Bettina Fischer[3], Sarah J. Bray[4], Jacques Colinge[1] and Alexandre Djiane[1,*]

ABSTRACT

Aggressive neoplastic growth can be initiated by a limited number of genetic alterations, such as the well-established cooperation between loss of cell architecture and hyperactive signaling pathways. However, our understanding of how these different alterations interact and influence each other remains very incomplete. Using *Drosophila* paradigms of imaginal wing disc epithelial growth, we have monitored the changes in Notch pathway activity according to the polarity status of cells (*scrib* mutant). We show that the *scrib* mutation impacts the direct transcriptional output of the Notch pathway, without altering the global distribution of Su(H), the Notch-dedicated transcription factor. The Notch-dependent neoplasms require, however, the action of a group of transcription factors, similar to those previously identified for Ras/*scrib* neoplasm (namely AP-1, Stat92E, Ftz-F1 and basic leucine zipper factors), further suggesting the importance of this transcription factor network during neoplastic growth. Finally, our work highlights some Notch/*scrib* specificities, in particular the role of the PAR domain-containing basic leucine zipper transcription factor and Notch direct target Pdp1 for neoplastic growth.

KEY WORDS: Notch signaling, *Drosophila*, Epithelial polarity, Neoplasia

INTRODUCTION

Epithelial cells represent the basic unit of many organs. They are polarized along an apico-basal (A/B) axis, a feature crucial for many aspects of their biology. A/B polarity is controlled by the asymmetric segregation of highly conserved protein complexes such as the Scrib/Dlg/Lgl complex (Bilder et al., 2003; Coopman and Djiane, 2016; St Johnston and Ahringer, 2010). The far-reaching effects of A/B polarity is epitomized by the observation that many tumors of epithelial origin exhibit impaired polarity, and that several viral oncoproteins target polarity complexes (Banks et al., 2012; Huang and Muthuswamy, 2010).

Studies in human cell lines and in animal models have also suggested that polarity alterations play a role in tumor formation. For instance, mutations in the baso-lateral determinant *SCRIB* have been shown to control proliferation and invasion in MCF-10A human mammary cells (Cordenonsi et al., 2011). Similarly in *Drosophila*, *scrib*, *dlg* or *lgl* mutations result in multilayered overgrowth of larval epithelial imaginal discs (Bilder et al., 2003; Bunker et al., 2015). However, this uncontrolled growth is at least partly achieved because larvae exhibiting *scrib* mutations fail to undergo proper metamorphosis and imaginal discs grow for an extended period. Indeed, *scrib* mutant cells actually grow slower than wild-type cells and are eliminated by wild-type neighbors (Cordero et al., 2010; Igaki et al., 2009, 2006; Ohsawa et al., 2011). Interestingly, this is reversed when additional mutations are introduced, such as overexpression of the BTB/POZ chromatin remodelers Abrupt or Chinmo (Doggett et al., 2015; Turkel et al., 2013) or the constitutive activation of signaling pathways (e.g. Ras or Notch), converting *scrib* mutant cells into aggressive, invasive and hyperproliferative cells (Brumby and Richardson, 2003; Pagliarini and Xu, 2003). Similar observations have been reported in mouse, where Notch or Ras activation and *Par3* depletion cooperate to generate aggressive neoplasms in mouse mammary glands (McCaffrey et al., 2012; Xue et al., 2013).

The Notch pathway is a highly conserved cell-signaling pathway that is misregulated in several cancers (Ntziachristos et al., 2014; Ranganathan et al., 2011). Upon activation, Notch receptors undergo two proteolytic cleavages to release their intracellular domain or NICD, which enters the nucleus, binds to the Notch pathway-specific transcription factor CSL [Rbpj in mammals; Suppressor of Hairless, Su(H) in *Drosophila*], and converts it from a repressor to an activator to turn on the transcription of specific target genes (Bray, 2016). These Notch direct target genes differ depending on the cell type and account for the variety of outcomes triggered by Notch activity. Increased Notch activity has been associated with several epithelial cancers, such as non-small-cell lung carcinomas (Maraver et al., 2012; Ntziachristos et al., 2014), but in animal models the sole increase in Notch activity either promotes differentiation or only results in benign over-proliferation (hyperplasia) (Brumby and Richardson, 2003; Djiane et al., 2013; Fre et al., 2005; Ho et al., 2015; McCaffrey et al., 2012). However, as mentioned previously, Notch pathway activation cooperates with loss of polarity to generate invasive neoplasms (Brumby and Richardson, 2003; Ho et al., 2015; McCaffrey et al., 2012; Pagliarini and Xu, 2003).

So, although the cooperation between loss of cell architecture and hyperactive signaling pathways is well established, the underlying mechanisms remain poorly understood. It could merely reflect an additive effect whereby the consequences of both events combine. Alternatively, it could indicate a more profound integration within epithelial cells whereby these two events impact on each other to generate unique new behaviors. Using *Drosophila* paradigms of

[1]IRCM, Inserm, University of Montpellier, ICM, Montpellier, France. [2]IRCM, Inserm, University of Montpellier, ICM, CNRS, Montpellier, France. [3]Department of Genetics, University of Cambridge, Cambridge CB2 3EH, UK. [4]Department of Physiology Development and Neuroscience, University of Cambridge, Cambridge CB2 3DY, UK.

*Author for correspondence (alexandre.djiane@inserm.fr)

P.L., 0000-0002-2785-7843; D.K., 0000-0001-9723-7204; S.J.B., 0000-0002-1642-599X; J.C., 0000-0003-2466-4824; A.D., 0000-0001-6210-2713

Handling Editor: Thomas Lecuit
Received 17 August 2021; Accepted 17 December 2021

Development (2022) 149, dev200110. doi:10.1242/dev.200110

imaginal wing disc epithelial growth, we have monitored the changes in Notch pathway activity according to the polarity status of cells and show that epithelial polarity changes directly impact the transcriptional output of the Notch pathway. We further provide evidence that this Notch redirection is not mediated by new genomic binding regions for Su(H), but relies on the cooperation with Su(H) of a combination of transcription factors, such as Stat92E and basic leucine zipper (bZIP) factors, activity of which is triggered in response to JNK signaling during polarity loss, extending earlier reports on the cooperation between oncogenic Ras and polarity loss (Atkins et al., 2016; Davie et al., 2015; Külshammer et al., 2015; Uhlirova and Bohmann, 2006). Our work highlights in particular the role of the PAR domain-containing bZIP transcription factor Pdp1 for Notch-driven neoplastic growth.

RESULTS

Notch activation and *scrib* mutation cooperate to promote neoplastic growth

In order to gain insights into the mechanisms underlying neoplastic growth, we first characterized the effects of Notch activation and *scrib* mutation-mediated epithelial polarity impairment on wing disc growth. Using precisely controlled *Drosophila* larvae culture conditions (crowding and timing), we compared the phenotypes of wild-type (WT), NICD-overexpressing (N), *scrib* mutant (S) and NICD-overexpressing and *scrib* mutant (NS) third instar wing imaginal discs at 6 days after egg laying at 25°C. These different paradigms are shown in Fig. 1A-D. For clarity, in all figures N will be shown in green, S in red and NS in blue. Reproducing our previous observations (Djiane et al., 2013), N discs overgrew compared with WT discs, but remained as monolayered epithelia, and represent a paradigm of hyperplastic-like growth (Fig. 1A,B). S discs were smaller than WT discs, but grew as an unstratified mass of cells. These discs, however, showed an extensive expression of the JNK signaling target Mmp1 (Fig. 1C), a metalloprotease implicated in the digestion of the extracellular matrix, indicative that *scrib*$^{-}$ cells activate JNK signaling and are prone to invasiveness (Igaki et al., 2006; Uhlirova and Bohmann, 2006). It is noteworthy that S larvae did not pupariate and if left to grow for longer the S discs ultimately developed as massive overgrowths with very disrupted epithelial polarity, that invaded and fused with neighboring tissues, such as other discs (Bilder et al., 2003). Strikingly, NS discs combined aspects of N and S discs. They were overgrown, like N discs, but also expressed high levels of Mmp1, like S discs (Fig. 1D). These discs grew as multilayered tissues and were able to invade the surrounding tissues, such as haltere discs, and represent, therefore, a paradigm for neoplastic-like growth.

Neoplastic and hyperplastic discs have different transcriptomes

The context of the *scribble* mutation converts the Notch-based *Drosophila* wing disc hyperplasia into a paradigm of neoplastic growth. Although the cooperation between activated Ras and *scrib* mutations has been studied extensively, mainly in the eye imaginal disc (Atkins et al., 2016; Cordero et al., 2010; Davie et al., 2015; Igaki et al., 2009; Katheder et al., 2017; Pagliarini and Xu, 2003; Toggweiler et al., 2016; Wu et al., 2010), less attention has been given to the cooperation between polarity loss and other activated pathways, such as Notch or Hedgehog (Brumby and Richardson, 2003; Pagliarini and Xu, 2003), preventing an evaluation of how general the studies on Ras signaling are to neoplasia development.

First, we carried out RNA sequencing (RNA-Seq) of the transcriptomes of the different genetic conditions to identify the differently expressed genes in N, S and NS compared with WT controls (using DESeq with adjusted *P*-value for multiple testing <0.05; Fig. 1E,F, Table S1; Anders and Huber, 2010). The numbers were broadly similar in the different conditions: N (503 upregulated; 663 downregulated), S (757 upregulated; 1029 downregulated) and NS (1003 upregulated; 991 downregulated). Semi-quantitative qRT-PCR validated the transcriptional changes in a subset of genes. For instance, *E2f1*, *Sdr* and *mxc* were activated only in N discs, whereas *Act87E* and *Wnt10* were activated only in NS. In addition, *Ets21C*, *ftz-f1* and *Atf3* were upregulated in all conditions (Fig. S1A). Comparing these data with previously published transcriptomes on similar or related genetic backgrounds revealed significant overlap, validating our experimental approaches. For instance, 174/503 upregulated, and 285/663 downregulated genes in N were also detected in our previous analysis using dual-color differential expression arrays (significant overlap *P*=1.11e−273, hypergeometric test; Djiane et al., 2013). Similarly, 676/757 upregulated genes in S were identified in a previous analysis of *scrib*-depleted discs (significant overlap *P*=4.90e−193; Bunker et al., 2015).

Gene ontology (GO) term analysis (*P*<0.05) confirmed that, as expected from their genetic composition, genes in the Notch signaling pathway (GO:0007219) were over-represented in the N and NS transcriptomes, whereas genes affected by changes in A/B polarity (GO:0045197; GO:0019991) were enriched in the NS and S transcriptomes (Fig. 1G). This analysis revealed potential common behaviors shared by N and NS, in particular signs of increased proliferation, consistent with the overgrowth phenotypes [e.g. ‘mitotic cytokinesis’ (GO:0000281) and ‘mitotic spindle organization’ (GO:0007052)], or behaviors shared between NS and S, such as those related to cell migration [e.g. ‘border follicle cell migration’ (GO:0007298)] or cellular stress [e.g. ‘response to starvation’ (GO:0042594); ‘response to endoplasmic reticulum stress’ (GO:0034976)] (Fig. 1G). Notably, several GO categories were enriched specifically in NS, including ‘mitotic G1/G2 DNA damage checkpoint’ (GO:0031571/GO:0007095), or ‘glutathione metabolic process’ (GO:0006749). These results argue that the combined Notch activation and polarity loss promoted the emergence of new cell behaviors and responses, in particular related to DNA-damage responses (Fig. 1G,H).

Hyperplasia and neoplasia harbor different Notch direct target networks

This raises the question of how the defects in *Notch* and in *scrib* cooperate to produce these transcriptional consequences. One particularly important aspect is how the Notch pathway is affected by the *scrib* mutation. Many signaling pathways, such as Ras, branch and act through several transcription factors and/or combine nuclear and cytoplasmic responses, making the analysis of how they are affected by the *scrib* mutation complicated. As the Notch pathway is extremely direct and the major, if not unique, output of Notch signaling is transcriptional activation (Bray, 2016), it offers a unique opportunity to investigate how the *scrib* mutation could potentially affect Notch signaling in NS cooperation. We thus decided to monitor the genes directly activated by Notch and study whether the Notch direct program (Notch direct targets, NDTs) is affected by the *scrib* mutation.

Genes that are directly regulated by Notch (NDTs) should have a transcription complex containing Su(H) bound at their regulatory regions (Djiane et al., 2013). To identify potential NDTs in N and NS, we thus monitored the genomic regions occupied by the Su(H) transcription factor by genome-wide chromatin immunoprecipitation

Development (2022) 149, dev200110. doi:10.1242/dev.200110

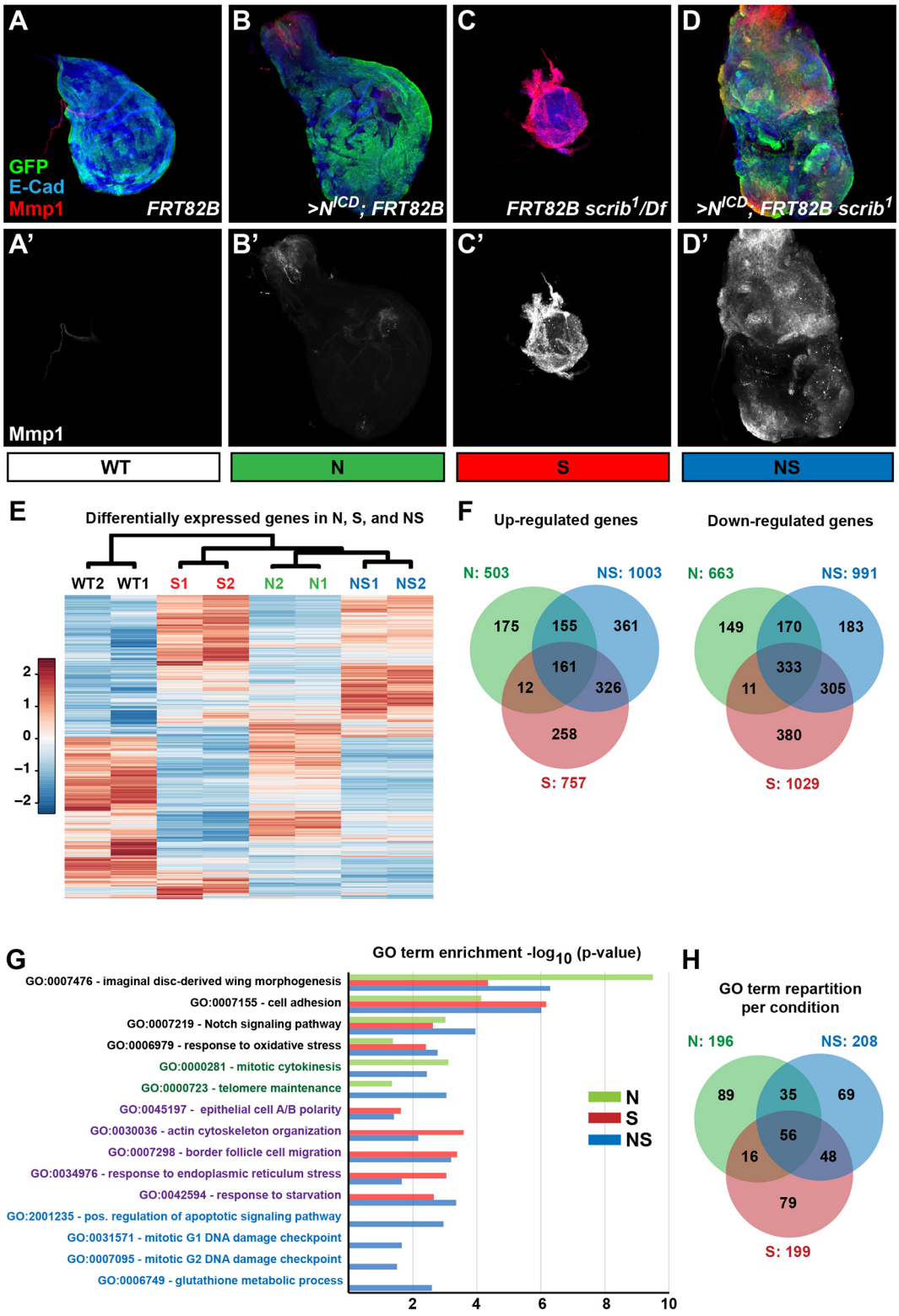

Fig. 1. Notch-based growth paradigms in *Drosophila* wing discs. (A-D) Third instar wing imaginal discs at precisely 5 days after egg-laying either wild type (WT; A), overexpressing activated Notch (N; B), mutant for *scrib* (S; C), or combining overexpressed Notch and *scrib* mutation (NS; D), and marked for E-Cadherin (Shg; E-Cad; blue) and Mmp1 (red). (A,A′,B,B′,D,D′) MARCM clones (positively marked by GFP; green) of the indicated genotypes: expressing only GFP (A,A′; WT), expressing NICD and GFP (B,B′; N), and expressing NICD and GFP and mutant for *scrib* (D,D′; NS). (C,C′) Discs fully mutant for *scrib*. (E,F) Differentially expressed genes compared with WT in the different growth paradigms, N (green), S (red) and NS (blue), identified by RNA-Seq. This color code, green for N, red for S, and blue for NS is used in all figures. (E) Heatmap of gene expressions after unsupervised clustering. (F) Venn diagrams of upregulated and downregulated genes in N, S and NS. (G) Enrichment diagram as measured by adjusted *P*-value for selected GO terms and represented as bars for N (green), S (red) and NS (blue). The color of the GO terms reflects whether they are shared or specific: shared by all (black), common to N and NS (dark green: mix of green and blue), common to S and NS (purple: mix of red and blue). (H) Venn diagram showing the domains of overlap of GO terms identified (significantly enriched) in N, S and NS.

Development (2022) 149, dev200110. doi:10.1242/dev.200110

(ChIP) (Fig. 2A; Table S2). These overlapped significantly with our previous analysis of Notch-induced overgrowth, suggesting that we had captured all the robust regions of Su(H) enrichment.

Strikingly, there was a strong overlap in the Su(H)-bound regions between N and NS conditions: almost all NS Su(H) peaks (416 out of a total of 464) overlapped with peaks present in N discs. This implies that the vast majority of Su(H) binding peaks in NS were also present in N (Fig. 2C, Fig. S1C). The overlap was also noteworthy between N and S peaks (447/554 S peaks overlapping with N peaks; Fig. 2C, Fig. S1C). These results suggest that in NS neoplastic discs, a minority of Su(H) peaks represent new binding regions compared with hyperplastic N discs, and that the new NS behaviors are not the consequence of general re-distribution of the Notch-specific transcription factor Su(H).

In order to estimate the programs specifically activated by Notch in N and NS, we then intersected the transcriptomic data with the Su(H) ChIP data, on the basis that upregulated genes located within 20 kb of a Su(H) peak were likely NDTs. Using this approach, we identified similar numbers of NDTs in N (176) and NS (174) (Fig. 2A,B, Table S3). Again, there was substantial overlap with previous data,

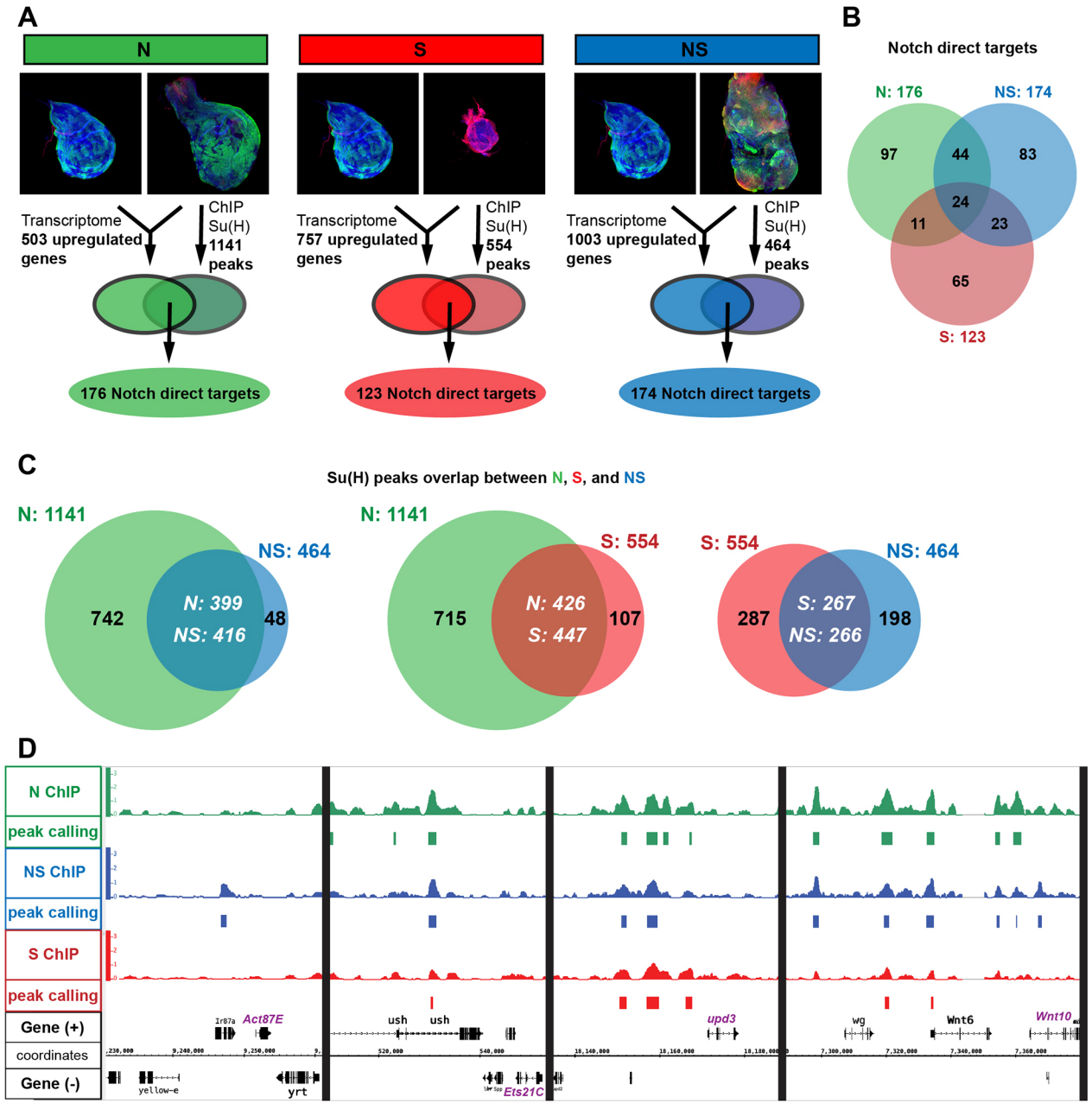

Fig. 2. Polarity loss redirects the transcriptional output of Notch during neoplastic growth. (A) Experimental set-up to identify NDTs – genes upregulated in N, S or NS (transcriptomic) and located within 20 kb of a Su(H)-binding site (ChIP). (B) Venn diagram showing the overlap of NDTs in N, S and NS, showing core Notch responses, but also significant condition-specific NDTs. (C) Overlap of the Su(H)-binding sites identified by ChIP in N, S and NS, showing that almost all S and NS Su(H) peaks are also found in N. The overlap is shown in white. Numbers are slightly different because in the Su(H) peaks calling protocol, in some rare cases, some peaks can be split between conditions whereby one peak in one condition would overlap with two peaks in the other. (D) Genome Viewer snapshots of several NDTs (shown in purple), such as the NS-specific *Act87E* and *Wnt10* (but also *yellow-e* and *Ir87a*), the common *Ets21C*, and the N/NS NDT *upd3*. For each condition, the Su(H) ChIP enrichment is shown in the upper lane, and the Su(H) peaks identified are represented by the blocks underneath.

Development (2022) 149, dev200110. doi:10.1242/dev.200110

with 64/176 NDTs in the N condition being identified in our previous study (significant overlap P=5.89e−96, hypergeometric test; Djiane et al., 2013). When the N and NS scenarios were compared, 68 genes were common to both and thus represent core NDTs in wing disc overgrowth. However, a significant proportion of NDTs appeared to be specific for each condition: 108 for N, 106 for NS. Of the 106 NS-specific NDTs, 23 were also NDTs in S. Indeed, affecting only polarity with the *scrib* mutation already alters the Notch program (123 NDTs in S). But the difference between N and NS cannot be explained by this S contribution alone as it concerns only 23 NDTs, and, taking all comparisons into account, 83 genes appear to be true NS-specific NDTs (Fig. 2B). Only a minority were associated with new Su(H)-binding regions: around the *87E* locus (*yellow-e3*, *yellow-e*, *Ir87a* and *Act87E*) and the *94A* locus (*CG18596*, *CG7059*, *CG13857* and *CG13850*), but also next to the *vito*, *cdi*, and *REG* genes (see Table S3).

These results indicate that although a core Notch response can be identified in overgrowing wing discs (68 genes; Fig. 2B), the loss of polarity affected the direct transcriptional output of the Notch signaling pathway: 108 NDTs specific to N were lost and 83 NDTs specific to NS were gained. Importantly, these changes in the Notch program are only marginally mediated by a redeployment of the transcription factor Su(H): 11/83 NS NDTs correspond to NS-specific Su(H) enrichment.

Neoplastic overgrowth is not mediated by the new NS-specific Su(H) regions

Using the NDT datasets, we sought to identify the factors that are required for the transition from N hyperplastic to NS neoplastic growth.

First, we decided to investigate the contribution of the DNA-damage response. Indeed, several NS-specific NDTs are implicated in DNA-damage response (e.g. *p53*, *His2Av*) and the GO analysis highlighted categories specific to NS related to 'response to oxidative stress' (GO:0006979), 'cellular response to gamma radiation' (GO:0071480) and 'DNA damage checkpoints' (GO:0031571/0007095). We thus investigated whether interfering with such pathways could block the growth and invasiveness of NS tissues. To perform these genetic tests, we generated a stable fly line that overexpressed NICD and *scrib* RNAi together with a green fluorescent protein (GFP) marker under the *Bx-Gal4* driver (driving expression in the pouch of the larval wing discs; *Bx>NS*), and monitored the size of the overgrowth (GFP-positive tissue), and its invasiveness potential (Mmp1-expressing cells; Fig. 4A-A″).

Blocking the oxidative stress response by overexpressing the reactive oxygen species (ROS) sponge CAT and SOD did not have any significant effect on the NS overgrowth or the expression of Mmp1 (Fig. 4E,F). Similarly, expression of RNAi or dominant-negative forms of the severe DNA-damage major effector and NS-specific NDT *p53* could not modify the NS overgrowth phenotype (Fig. 4E,F). Although we cannot exclude the possibility that the tools used here were not strong enough, these results suggest that, even though activated in NS tissues, oxidative stress and p53-mediated DNA-damage responses were either not required to fuel NS growth, or that they could compensate for each other converging ultimately on an as-yet-unidentified core response promoting NS growth.

Second, we turned our attention to the NS-specific NDTs associated with unique Su(H) binding. Indeed, even though the emergence of new Su(H) binding is not the main mechanism driving the NS-specific Notch program, it remains possible that these loci and the genes associated are functionally important for the NS neoplastic behavior. We thus investigated whether interfering with these 11 NS-specific NDTs could block the growth and invasiveness. Knocking down by RNAi the expression of the different genes associated with the *87E* locus (*yellow-e3*, *yellow-e*, *Ir87a* and *Act87E*) and with the *94A* locus (*CG18596*, *CG7059*, *CG13857* and *CG13850*) did not have any significant effect on NS overgrowth. Similarly, we could not detect any change in NS tumor overgrowth after RNAi-mediated knockdown of *cdi*, *REG* and *vito* (data not shown). It should be noted, however, that for several genes only one RNAi could be tested with the potential caveat of insufficient knockdown efficiencies (Xia et al., 2021). However, our results suggest that these NDTs associated with NS-specific Su(H) binding are not required, at least individually, for NS overgrowth. But even though not strictly required, their overexpression might still contribute, redundantly with other factors, to the overall NS neoplastic behaviors. Of these particular NS NDTs, *Act87E*, associated with the new Su(H) peak at locus *87E* (Fig. 2D), was the most robustly upregulated in NS (Table S1, Fig. S1A). When overexpressed in wild-type wing disc, or in combination with activated Notch, Act87E led to robust expression of the metalloprotease and JNK target Mmp1, and cell delamination. Act87E also induced robust expression of the effector caspase Dcp-1 (Fig. S2). *Act87E* might thus represent a stress gene activated in NS that initiates cell delamination and ultimately cell death, but whose role is not necessary and/or redundant with other NS-activated genes.

Identification of the transcriptional networks in the different growth paradigms

Taken together, our results indicate that even though the *scrib* mutation was able to change the transcriptional output of the Notch pathway, the difference between N and NS is not due to a redeployment of Su(H) to activate new NS-specific genes. Therefore, other factors brought upon by the *scrib* mutation must influence gene expression.

We thus sought to identify transcriptional factors that could account for the cooperation between Notch and polarity loss. We used iRegulon software (Janky et al., 2014; Verfaillie et al., 2015) to identify the transcription factors likely to co-regulate the genes identified in N, S or NS. Previous usage of iRegulon on *RasV12/scrib*$^{-}$ overgrown third instar larval discs, highlighted an 'oncogenic module' comprising the Hippo pathway terminal effectors Yki and Sd, the JNK pathway regulated AP-1 factors [in particular, Atf3, Kay and CEBPG (Irbp18)], the Jak/Stat pathway, Myc, Crp and Ftz-F1 (Atkins et al., 2016; Davie et al., 2015; Külshammer et al., 2015).

Implementing iRegulon on our step-wise Notch-based paradigms allowed us to (1) identify transcriptional modules unique or shared between polarity loss only (S), proliferation only (N) and proliferation plus invasiveness (NS), and (2) assess the conservation of the 'oncogenic module' identified previously with Ras in a Notch-driven neoplastic paradigm. We performed these analyses feeding iRegulon either with the lists of upregulated genes in N, S and NS (Fig. 3, Table S4) or with the lists of NDTs (Fig. S3, Table S5). We decided to focus our analyses on the upregulated genes here because the overexpressed NICD triggers transcriptional activation (Bray, 2016) and downregulated genes might thus represent very indirect effects of the cooperation. Modules identified are presented as Venn diagrams (Fig. 3, Fig. S3) highlighting the common and specific transcription factor modules that were identified as likely master regulators of the transcriptional changes in the different conditions. Feeding either upregulated genes (Fig. 3) or NDTs (Fig. S3) identified similar

Development (2022) 149, dev200110. doi:10.1242/dev.200110

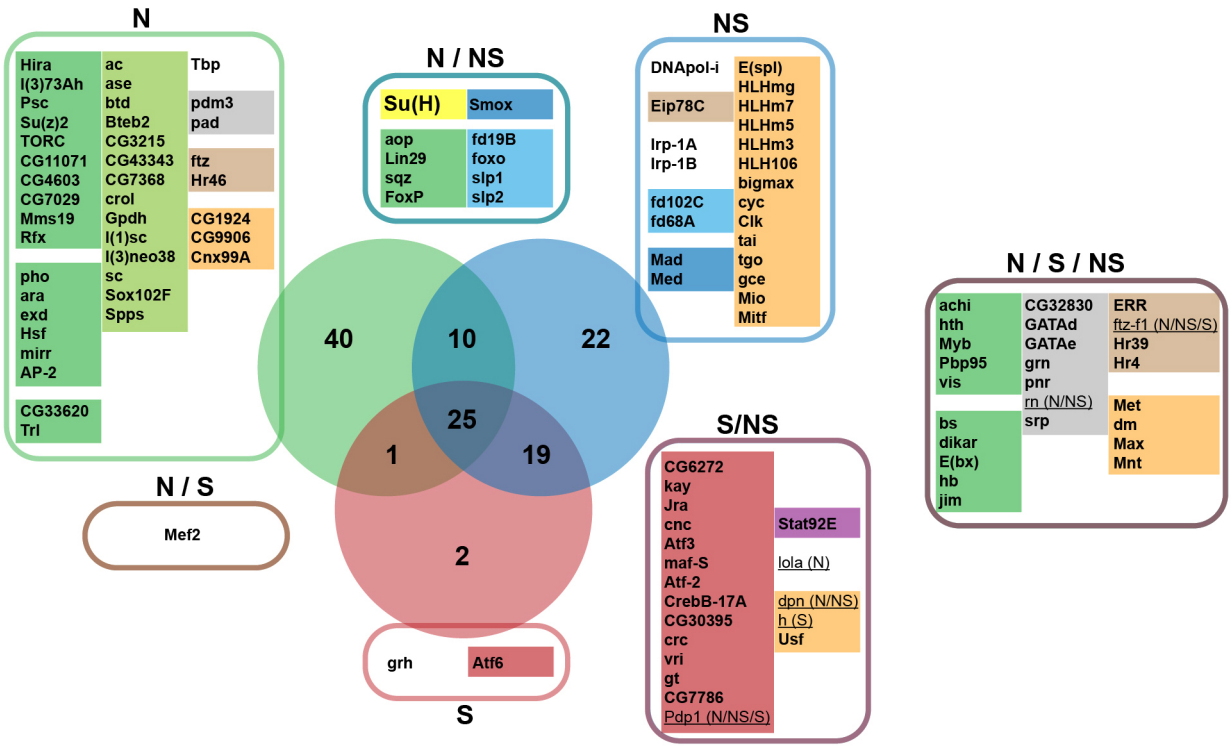

Fig. 3. Identification of potential transcriptional modules mediating N, S and NS growth. Venn diagrams of significant transcription factors (TFs) identified by iRegulon as potential key mediators for the expression of upregulated genes in N (green circle), S (red circle) and NS (blue circle). Fed with lists of co-regulated genes, and analyzing the genomic features in the vicinity of the transcription start sites of these genes, iRegulon identifies potential groups of TFs and DNA-binding factors that are enriched in the dataset of regulatory sequences, and could thus represent potential mediators of the N, S and NS transcriptomes. For each condition, TFs were identified as part of 'regulons' or a group of TFs that could potentially together regulate the expression of subsets of the transcriptome. Taking only the TFs corresponding to the significant regulons identified in N, S and NS, the shared and unique potentially regulating TFs are here presented in the different colored boxes. In each box, TFs were then grouped according to their molecular family (suggesting similar binding motifs on the DNA), and marked by a color-coded box: for instance, bZIP TFs in light red, or the nuclear receptors in brown. The molecular family color code was not respected for the green and light green groups which correspond to very diverse 'regulons' that appear linked to epigenetic chromatin regulators/remodelers. For the complete list of regulons identified in each condition, and the nature of TFs and DNA binding proteins in each regulon, see Table S4. Numbers in the Venn diagram represent the number of TFs identified. TFs that are also NDTs and which could participate in feed-forward loops are underlined (with their NDT condition in parentheses). See also Fig. S3 for the iRegulon analyses of the NDTs, and detailed lists of both iRegulon analyses in Table S5.

modules, indicating that the Notch pathway condition-specific transcription programs are mediated, at least in part, by transcription factors that broadly affect the whole transcriptome. This is likely also true for other neoplastic paradigms such as Ras, although this remains to be established. Importantly, iRegulon identified the Notch pathway-dedicated transcription factor Su(H) in the N and NS transcriptomes.

First, focusing on NS, which most resembles the *RasV12/scrib*$^{-}$ paradigms, our analysis identified the same major nodes and the transcription factors associated with the 'oncogenic module' as described previously for the *RasV12/scrib*$^{-}$ models: AP-1 basic leucine zipper factors related to stress kinase signaling; Stat92E of the Jak/Stat pathway; the nuclear receptor Ftz-F1; and basic helix-loop-helix (bHLH) factors of the Myc family. In the NS transcriptome, we also identified a contribution of the E(spl) bHLH transcriptional repressors. E(spl)-HLH genes are canonical Notch targets, and they are robustly upregulated in N and NS, in particular *E(spl)mγ-HLH*.

The iRegulon analyses also suggested that the AP-1 bZIP and Stat92E signatures in NS are contributed by S, because they are also detected in the S transcriptomes, whereas the Su(H) signature is contributed by N. Finally, iRegulon identified a signature for the Polycomb chromatin silencers specifically in N. Such factors include Pho, a zinc-finger protein that binds to Polycomb responsive elements (PREs) and recruits Polycomb complexes, and the three Polycomb repressor complex 1 (PRC1) components Psc, Su(z)2 and l(3)73Ah. Recently, PRC1 has been associated with specific and unexpected transcriptional activation at larval stages, raising the possibility that in N, such genes, normally repressed at embryonic stages, become active (Loubiere et al., 2020). However, the exact contribution of Polycomb factors, and whether they are actually involved in gene activation upon Notch activation, or whether the 'Polycomb' module of iRegulon merely indicates gene de-repression, has not been addressed formally in this study.

A polarity-loss response required for NS

In order to validate the functional relevance of the transcription factors identified in the Notch-driven neoplastic growth, we then investigated whether their depletion by RNAi could alter the growth and invasiveness of the NS tissue, using the *Bx>NS* fly line described previously. We first focused our analysis on the factors associated with the 'oncogenic module'.

We confirmed earlier reports that blocking JNK activity by the overexpression of a JNK dominant-negative construct strongly abolishes NS-driven growth (GFP-positive tissue size; Fig. 4B,B′,E) and invasiveness (Mmp1 expression; Fig. 4B,B″,F). As shown in the *RasV12/scrib*$^{-}$ paradigms, RNAi mediated knockdown of the Jak/Stat pathway terminal transcription factor

Development (2022) 149, dev200110. doi:10.1242/dev.200110

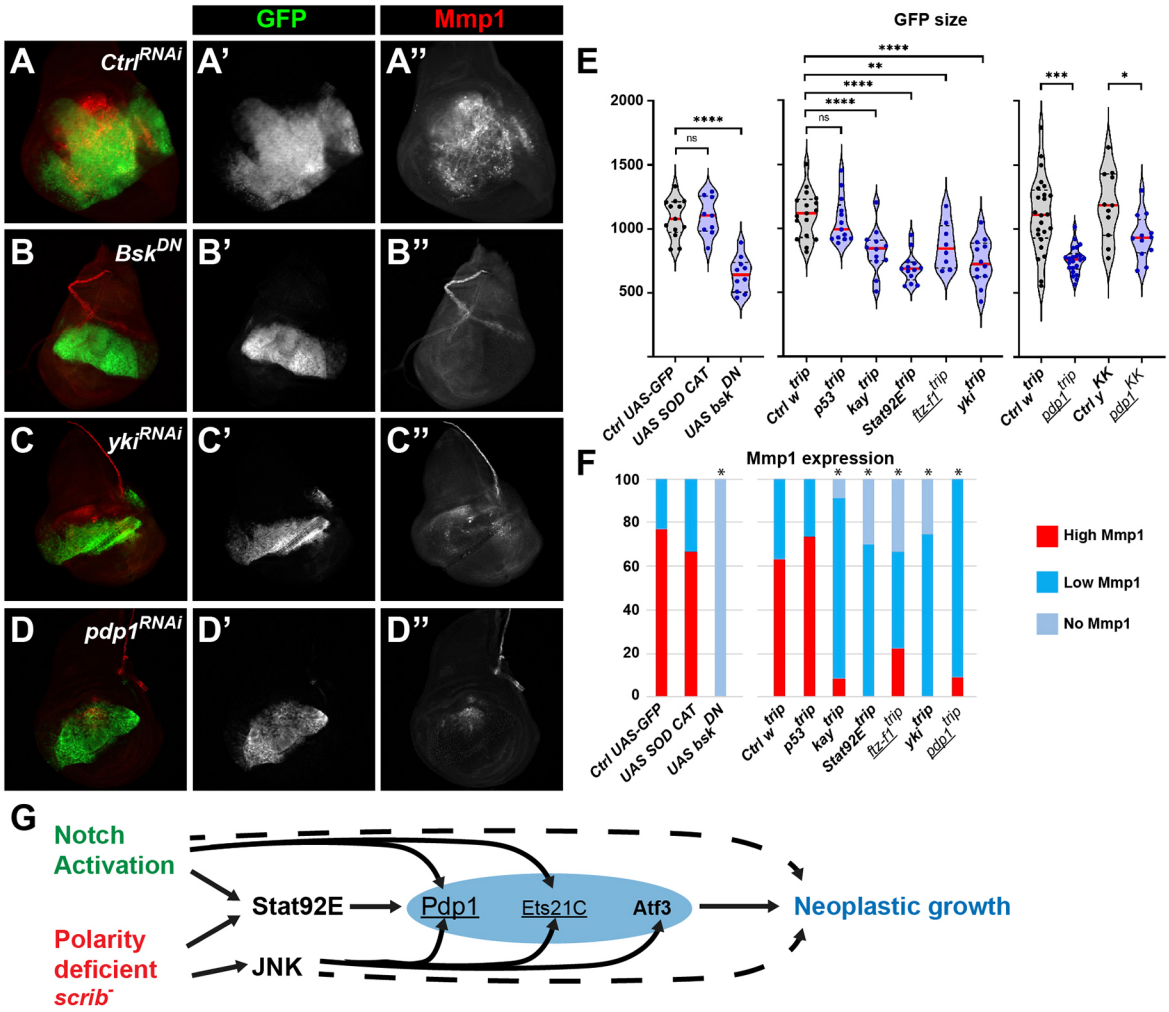

Fig. 4. Neoplastic growth is mediated by an AP-1/Stat/Yki/Ftz-f1 module and by a diverse network of bZIP transcription factors, including Pdp1. (A-D″) Third instar wing imaginal discs expressing GFP, an activated form of Notch (NICD) and an RNAi for *scrib* under the control of the *Bx-Gal4* driver (dorsal wing pouch) and stained for GFP (green; white in A′-D′) to assess tissue overgrowth and for Mmp1 (red; white in A″-D″) to assess tissue invasiveness. Discs also expressed under *Bx-Gal4* control either *UAS Bsk DN* (B) or the indicated RNAi constructs: *w[HMS00045]* (A; Ctrl), *yki[HMS00041]* (C), *Pdp1[HMS02030]* (D). Representative discs are shown. (E) Quantification of the overgrowth of the GFP territory in the indicated genotypes. Results are shown as violin plots of total GFP area measured in arbitrary pixels. Controls for each experiment are shown in gray. Statistical tests: ANOVA (left and middle graphs) or unpaired, two-tailed *t*-test (right graph); n.s., non significant; **P*<0.05; ***P*<0.01; ****P*<0.001; *****P*<0.0001. For more details of RNAi lines either from the TRiP collection (labeled with 'trip' superscript) or from the Vienna collection (labeled with 'KK' superscript) are provided in supplementary Materials and Methods. (F) Quantification of Mmp1 staining intensity in the indicated genotypes. Results are shown as the percentage of discs classified as the following categories: high Mmp1 staining intensity (red, similar to that shown in A″), low Mmp1 staining intensity (blue, similar to that shown in D″), or no Mmp1 staining (light blue, similar to that shown in B″). Statistical test: chi-square test for trend or Fisher's exact test; **P*<0.05. (G) Feed-forward model of the cooperation between Notch and polarity loss during wing imaginal disc neoplastic growth. In E-G, the Pdp1, Ets21C and Ftz-f1 NDTs are underlined.

Stat92E, and to a lesser extent *ftz-f1* (Atkins et al., 2016; Davie et al., 2015; Külshammer et al., 2015; Toggweiler et al., 2016), strongly suppressed both growth (GFP) and invasiveness (Mmp1; Fig. 4E,F). Unlike the RasV12 models, we did not identify in the different iRegulon analyses of the N, S and NS transcriptomes any particular enrichment for Sd (also known as TEAD), the transcriptional factor mediating the effect of Yki and of the Hippo pathway-mediated growth in wing discs. However, impairing Yki activity (through RNAi-mediated knockdown) strongly suppressed NS neoplastic behaviors (Fig. 4C-C″,E,F).

Taken together, these results suggest that, independently of the oncogenic drivers, Ras or Notch, relatively similar tumorous transcriptional networks (AP-1/Yki/Stat/Ftz-f1) are put in place during their cooperation with polarity loss (Atkins et al., 2016; Davie et al., 2015; Hamaratoglu and Atkins, 2020; Külshammer et al., 2015). Given that these nodes were also identified in the S transcriptome, we suggest that they represent a polarity-loss module cooperating with oncogenic signaling pathways Ras or Notch, and likely other pathways, such as Hh, as was initially reported (Brumby and Richardson, 2003).

The PAR domain-containing transcription factor Pdp1 is required for neoplastic growth

A striking feature of the iRegulon analyses was the NS/S JNK module, which contained classic bZIP transcription factors, such as Jun or Fos. These factors are involved in complex homo- and hetero-dimers mediating cellular responses to different stresses such as DNA damage and oxidative stress (Reinke et al., 2013), and their binding specificities remain difficult to tease apart. Atf3 has recently been shown to control the expression of genes involved in

Development (2022) 149, dev200110. doi:10.1242/dev.200110

the maintenance of epithelial polarity, and to be specifically activated in polarity-deficient cells and required in the *RasV12/scrib*$^{-}$ overgrowth model (Atkins et al., 2016; Donohoe et al., 2018). Strikingly, among the different bZIP predicted by iRegulon to control the NS transcriptome, *Pdp1* is a direct Notch target (common in N, S and NS; Table S3, Fig. S4A), raising the interesting prospect that Pdp1 could act as feed-forward factor to promote neoplastic growth downstream of Notch.

Knocking down *Pdp1* using two independent RNAi lines, using the *Bx>NS* fly line, led to a robust reduction of tissue growth (as measured by total GFP area; Fig. 4D-E), and to a reduction in the intensity of Mmp1 staining (Fig. 4D,D″,F). Pdp1 (the homolog of hepatic leukemia factor, HLF) has previously been linked to mitotic cell cycle and growth (Reddy et al., 2006), and shown in the *RasV12/scrib*$^{-}$ paradigms to have only modest effects on invasion, but none on growth. In the context of Notch (NICD/*scrib*$^{-}$), the role of *Pdp1* appeared thus more essential, probably because *Pdp1* is a direct Notch target. But although *Pdp1* was required, was it sufficient to promote NS-like tumors? Overexpression of Pdp1 was sufficient to induce cell delamination and spreading, as evidenced by the increased Mmp1 staining and the spreading of GFP-positive cells on the anterior part of the disc (Fig. S4C-C″). Strikingly, the combined overexpression of NICD and Pdp1 resulted in high Mmp1 staining and a much wider GFP expression domain (compared with NICD or Pdp1 alone) indicative of invasive and/or delaminating cells extending anteriorly (Fig. S4C-E). Even though these features reproduce in part some of the NS behaviors, in particular the increased Mmp1 staining, it should be noted that the discs overexpressing both NICD and Pdp1 appeared to grow poorly, unlike NS discs. Furthermore the Mmp1 upregulation upon NICD and Pdp1 overexpression was not restricted to the overexpressing cells, suggesting that the combination of NICD and Pdp1 in a restricted number of cells (under the control of the *Dpp-Gal4* driver) had non-autonomous effects both on growth and on Mmp1 expression (Fig. S4E, yellow arrowhead). Taken together, these results highlight the important role of Pdp1 in Notch-driven neoplasia (necessity), but show that the sole overexpression of Pdp1 in combination with NICD is not sufficient for optimal growth as observed in NS tumors, suggesting that the development of NS tumors rely on specific levels of Pdp1, together with the involvement of other transcription factors (e.g. Stat92E and Ftz-f1).

DISCUSSION

In this study, using Notch-driven paradigms of epithelial overgrowth in *Drosophila* wing discs, we describe the molecular mechanisms underlying the cooperation between Notch and polarity loss during neoplasia. We show that epithelial polarity alterations redirect the transcriptional outcome of the Notch signaling pathway, thus defining a specific set of new neoplastic Notch direct targets. We further show that this redirection occurs mainly on pre-existing Su(H)-bound regions rather than new ones. Finally, we show that, similar to what was previously described for Ras signaling (Atkins et al., 2016; Davie et al., 2015), the AP-1/Stat/Yki/Ftz-f1 transcription factors are required for the cooperation between Notch signaling and polarity loss during neoplastic growth.

Although cancer genomes exhibit multiple mutations in cancer cells, their functional interactions remain difficult to monitor and model. Neoplastic tissues, generated upon the combination of Notch pathway activation and polarity loss through *scrib* mutation, experience many cellular stresses: DNA-damage responses, but also endoplasmic reticulum and unfolded protein response, starvation or oxidative stresses. However, even though present, these different stresses, in particular oxidative stress and DNA damage, are not individually necessary in the context of polarity loss as blocking them or the cellular response they promote (by CAT/SOD overexpression, or inhibition of p53) did not significantly suppress the NS tumorous behaviors. These observations suggest that the different stress pathways activated during polarity loss are either not required for fueling growth (they are rather a consequence than a cause of neoplastic growth), or might act 'redundantly' to activate a common core response required for increased growth.

Although *Drosophila* and mouse models have demonstrated that overactive signaling pathways cooperate with epithelial polarity impairment to generate neoplastic growth (Brumby and Richardson, 2003; McCaffrey et al., 2012; Pagliarini and Xu, 2003; Xue et al., 2013), the vast majority of studies seeking to understand the underlying mechanisms have focused primarily on the cooperation between activated RasV12 and *scrib* mutants, especially in *Drosophila* (Atkins et al., 2016; Cordero et al., 2010; Davie et al., 2015; Igaki et al., 2009; Katheder et al., 2017; Pagliarini and Xu, 2003; Toggweiler et al., 2016; Wu et al., 2010). Importantly, the current study, investigating the cooperation between Notch and polarity, shows that many observations made for Ras can be extended to Notch, suggesting that the paradigms used are not specific to Ras but might represent a more general tumor growth paradigm. But, because the main, if not only, Notch pathway outcome is transcriptional, the NICD/*scrib*$^{-}$ model allowed the modes of cooperation to be studied in greater detail. The cooperation between Notch pathway activation and polarity loss led to a specific transcriptional program, and in particular the activation of new Notch direct targets. We showed that this was not the consequence of a general redeployment to new target gene loci of Su(H), the Notch pathway-dedicated transcription factor, ruling out one possible model for the oncogene/polarity cooperation. Thus, what could be the mechanisms controlling which genes were activated in the different conditions? All 'Notch'-activating transcriptional complexes comprise NICD, Mastermind and Su(H). Although no differences in overall levels of NICD and Su(H) could be detected by western blot (data not shown), they could be modified in different ways post-translationally leading to different Notch responses (e.g. core Notch response, N-only, NS-only). Indeed, recent reports point towards different post-translational modifications for Su(H) (Frankenreiter et al., 2021). However, whether they lead to different transcriptional programs, and whether they occur *in vivo* in the N and NS models, remain to be studied. Through the use of iRegulon, we demonstrated that the genes of the NS transcriptome, and most importantly the NS Notch direct targets, were enriched in their regulatory regions for elements corresponding to specific transcription factors, and in particular Stat92E or bZIP factors. The fact that similar transcription factor families were found in the overall group of upregulated genes and in the more limited subset of Notch direct genes suggests that the Notch output was controlled, at least in part, by factors that act more broadly on the genome. These analyses support a model in which polarity loss redirects the output of the Notch transcriptional program by the action of cooperating transcription factors. However, further work, such as detailed comparative ChIP analyses of the different factors in the different conditions, is required to establish this model firmly.

Although we demonstrated the involvement of a similar 'oncogenic module' as identified for the *RasV12/scrib*$^{-}$ neoplastic model (Atkins et al., 2016; Davie et al., 2015; Külshammer et al., 2015), there are specifics that are likely oncogene specific. First, unlike what was reported for *RasV12/scrib*$^{-}$ transcriptomes, Yki/Sd/TEAD modules were not found to be enriched in the different

Development (2022) 149, dev200110. doi:10.1242/dev.200110

Notch and *scrib*$^{-}$ transcriptomes. In the case of Ras, it has been shown that Yki activity can reprogram Ras by promoting the expression of the Ras pathway-specific regulators Capicua and Pointed to promote aggressive growth (Pascual et al., 2017). Both genes were either unaffected (*capicua*) or downregulated (*pointed*) in the NS Notch-driven neoplastic paradigm, suggesting that, even though Yki is clearly required (Fig. 4C), changes in the expression of *capicua* and *pointed* are unlikely to be mediators here. These differing results in the enrichment of Yki/Sd/TEAD motifs between Notch and Ras transcriptomes in the context of polarity loss might reflect the inhibitory effect Notch has on Yki activity in the wing pouch, in part through the action of *vestigial* (Djiane et al., 2014). Furthermore, in the NS transcriptome, we identified a contribution of the E(spl) bHLH transcriptional repressors, canonical Notch targets (Bray, 2016), which represents thus a Notch specificity. However, the fact that motifs for E(spl)-HLH repressors are found in the upregulated transcriptome of NS and not N could suggest that in NS the repressive ability of E(spl)-HLH factors is antagonized, further allowing higher expression of Notch targets. More precisely, our previous work identified many incoherent feed-forward loops in the N hyperplastic transcriptome, including through the action of E(spl) repressors (Djiane et al., 2013), which might thus be resolved in NS. It would be interesting to explore further the link between NS and E(spl)-HLH-mediated repression, but due to the high redundancy between the seven E(spl)-HLH factors (δ, γ, β, 3, 5, 7, 8) and Dpn, the requirement of E(spl)-HLH-mediated repression in Notch-driven neoplasia could not be formally tested.

By performing functional assays to identify the genes and processes required for NS tumor growth, we demonstrated that the Notch direct targets associated with '*de novo*' NS-specific Su(H) peaks were unlikely to be major contributors. We did show, however, that the bZIP PAR domain-containing factor Pdp1 is required for NS tumor growth and invasiveness. Su(H) is bound in the vicinity of Pdp1 in all wing discs set-ups, and in particular in N and NS, and Pdp1 represents a 'core' Notch target activated in all overgrowth conditions, albeit at higher levels in polarity-deficient conditions (Fig. S4A). Pdp1 is not only a Notch target, but also a Jak/Stat target, at least in the developing eye, and canonical tandem Stat92E putative binding sites are found in its second intron, although not overlapping with Su(H) binding, which is found in its first intron (Flaherty et al., 2009). Interestingly, Pdp1 is required for Stat92E phosphorylation and efficient Jak/Stat signaling (Baeg et al., 2005), suggesting that Notch might amplify Stat92E signaling during wing disc neoplastic growth, both through ligand expression (Upd ligands are Notch direct targets; this study; Djiane et al., 2013) and Pdp1 expression.

Although Pdp1 downregulation could suppress NS neoplastic growth, it was not as efficient as JNK inhibition, or Yki downregulation, suggesting that other factors in parallel to Pdp1 might be involved, such as the previously identified Atf3 (Donohoe et al., 2018), but also the other Notch direct target Ets21C (Fig. 2D; Külshammer et al., 2015; Toggweiler et al., 2016). Indeed, RNAi-mediated knockdown of *Atf3* or *Ets21C* partly suppressed *Bx>NS* tumor growth (GFP) and invasiveness (Mmp1; data not shown). This action of both Pdp1 and Ets21C suggest a feed-forward loop downstream of Notch that in the context of polarity loss and JNK activity promotes neoplastic growth (Fig. 4G). However, given that *Atf3*, *Pdp1* and *Ets21C* (but also *Ftz-f1*) are all upregulated in N hyperplastic conditions, their sole upregulation cannot be sufficient for neoplasia. The fact that Atf3 and Pdp1 iRegulon enrichments are not found in N (Fig. 3, Fig. S3) could indicate that, despite being upregulated in hyperplastic N, their transcriptional activities are hindered, or that one key cooperating factor enabling their action is missing. Further studies are thus required to test this possibility and study how, in the context of normal epithelial polarity, Notch activation prevents the action of Pdp1/Ets21C/Atf3, thus preventing the transition to neoplasia.

MATERIALS AND METHODS

Drosophila genetics

The different overgrowth paradigms were obtained by generating random clones in third instar wing discs at high frequency as previously published (Djiane et al., 2013). In brief, the *abxUbxFLPase; Act>y>Gal4, UAS GFP; FRT82B tubGal80* flies were crossed either to *FRT82B* (to generate control WT discs), or to *UAS-Nicd; FRT82B* (to generate hyperplastic N discs), or to *UAS-Nicd; FRT82B scrib1* (to generate neoplastic NS discs). *scrib1* represents a loss-of-function allele for the *scribble* gene. Because *scrib1* clones are eliminated in growing discs, the dysplasic S discs were obtained from *FRT82B scrib1/Df(3R)BSC752* third instar larvae. All crosses were performed at 25°C and carefully staged (by assessing time after egg laying and tube crowding).

For transcriptomic and ChIP analyses, discs were dissected from these carefully timed animals. N, S and NS overall larval body sizes were very similar to those of WT controls at days 5 and 6, suggesting that they grew normally during second and third instar larval stages. All animals with wing disc growth defects displayed pupariation delay: S and NS never pupated, whereas some (but not all) N animals eventually pupated at day 11 or 12 after egg laying (ael; normal time being 5 to 6 ael). These observations suggest that the main timing problem for N, S and NS was in the transition to pupa at 5-6 ael. By monitoring differences at day 6 ael, just after spiracle eversion (a classic landmark in developmental timing), we thus monitored differences just prior to the extension of larval life, and very far from the extreme that could be observed, suggesting that tissues would remain comparable.

For functional studies, neoplastic growth was obtained by driving *UAS-Nicd* and the *scrib* RNAi *P{TRiP.HMS01490}attP2* by the *Bx-Gal4* (pouch of larval wing discs). Modifications of the overgrowth phenotype and of the expression of the Mmp1 invasive marker were performed by crossing in F1 *Bx-Gal4, UAS GFP;; UAS Nicd, UAS scribHMS01490* to the desired *UAS RNAi* or control lines (*UAS white RNAi*, *UAS yellow RNAi* or *UAS GFP*), to ensure similar UAS load. See supplementary Materials and Methods for further details and a list of lines tested.

Information on gene models and functions, and on *Drosophila* lines available were obtained from FlyBase (Thurmond et al., 2019).

RNA extraction and RNA-Seq

RNA from 60 or 80 dissected third instar larva wing discs of WT, N, NS and S discs was extracted using TRIzol. Genomic DNA was eliminated using Ambion's DNA-free kit (AM1906). cDNA bank preparation were then performed from 1 µg of RNA and sequencing on an Illumina HisSeq 2000 by the Biocampus genomic facility MGX of Montpellier. After sequencing, reads obtained were filtered based on their quality (~40 million reads were kept per conditions). The reads were then aligned to the *Drosophila* dm6 genome by the ABIC facility in Montpellier producing a matrix of reads per gene and per condition. This matrix was then normalized and pair-wise differential expression was performed using DESeq (Anders and Huber, 2010). Other differential expression tools were tested, such as DESeq2 and edgeR with default parameters, but appeared either less stringent, or inadequate.

qPCR

qPCR was performed on biological triplicates on a Roche LightCycler 480, and fold change was estimated by the δδCT approach. See supplementary Materials and Methods for a list of primers used.

Su(H) ChIP

After dissection in 1× PBS, protein/DNA complexes from 60 wing discs (80 for S condition) were cross-linked with 1% formaldehyde for 10 min. The reaction was then quenched by 0.125 M glycine and washed three times in

Development (2022) 149, dev200110. doi:10.1242/dev.200110

PBS. Wing disc cells were resuspended in 50 µl Nuclear Lysis Buffer (20 mM Tris-HCl pH 8.1, 10 mM EDTA, 1% SDS). Lysates were sonicated on a Bioruptor (Diagenode), and diluted 1:10 in Immunoprecipitation Dilution Buffer (20 mM Tris-HCl pH 8.1, 2 mM EDTA, 0.01%SDS, 150 mM NaCl, 1%Triton X-100) and precleared with rabbit IgG (Sigma-Aldrich) and protein G Agarose (Santa Cruz Biotechnology). ChIP reactions were performed by incubating lysates overnight at 4°C with 1 ng goat anti-Su(H) (Santa Cruz Biotechnology, sc15813), and immunocomplexes were then isolated with Protein G Agarose for 2 h, washed twice with Wash Buffer 1 (20 mM Tris-HCl pH 8.1, 2 mM EDTA, 0.1%SDS, 50 mM NaCl, 1%Triton X-100) and twice with Wash Buffer 2 (10 mM Tris-HCl pH 8.1, 1 mM EDTA, 250 mM LiCl, 1% NP-40, 0.4% deoxycholic acid), before a de-crosslinking step at 65°C in 0.25 M NaCl. Samples were then treated with 0.2 mg/ml proteinase K and 50 mg/ml RNase A. The DNA was then purified on columns (Qiagen, 28106). ChIP efficiency was checked by qPCR normalized on input chromatin with primer couples corresponding to known strong binding sites of Su(H). See supplementary Materials and Methods for a list of primers used.

For whole-genome analysis, 1 µg double-stranded ChIP or input DNA (corresponding to 180 discs for each replicate) was labeled with either Cy3- or Cy5-conjugated random primers using the NimbleGen Dual Color kit. Both ChIP and input were co-hybridized to NimbleGen *D. melanogaster* ChIP-chip 2.1 M whole-genome tiling arrays in the NimbleGen hybridization station at 42°C for 16 h and then washed according to the NimbleGen Wash Buffer kit instructions. The data obtained were normalized using quantile normalization across the replicate arrays in R. Window smoothing and peak calling were performed using the Bioconductor package Ringo (Toedling et al., 2007) with a winHalfSize of 300 bp and min.probes=5. Probe levels were then assigned *P*-values based on the normalNull method, corrected for multiple testing using the Benjamini–Hochberg algorithm and then condensed into regions using distCutOff of 200 bp.

In order to determine the NDTs, ChIP and RNA-Seq results were compared: NDTs are defined as upregulated genes with Su(H) enrichment within 20 kb. As such, one Su(H) peak could be assigned to several upregulated genes consistent with its role in enhancer regions. The 20 kb window was chosen as it allowed the recovery of more than 85% of NDTs in our previous study, which was based on closest gene assignment irrespective of distance (Djiane et al., 2013).

GO term analyses

The lists of significantly regulated genes in the various comparisons were submitted to GO term enrichment analysis. We used the GO biological process (GOBP) ontology and applied hypergeometric tests (*P*-values) followed by Benjamini–Hochberg multiple hypothesis correction (q-values).

iRegulon analyses

In order to determine the likely transcriptional modules in our transcriptomic and NDTs datasets, we used the online tool iRegulon (http://iregulon.aertslab.org/) (Janky et al., 2014; Verfaillie et al., 2015), with the standard settings using the 6 K Motif collection (6383 PWMs) and a putative regulatory region of '10 kb upstream, full transcript and 10 kb downstream'. Importantly, these settings allowed the recovery of the 'positive control' Su(H) module.

Immunofluorescence

Antibody staining of wing imaginal discs was performed using standard protocols.

Briefly, larval heads containing the imaginal discs (LHs) were dissected in cold PBS and fixed for 20 min in 4% formaldehyde in PBS at room temperature (RT), before being rinsed three times (10 min each) in 0.2% Triton X-100 in PBS (PBT), and blocked in PBT+0.5% bovine serum albumin (PBTB) for 30 min at RT. LHs were then incubated overnight at 4°C with primary antibodies in PBTB. LHs were then rinsed three times (10 min each) in PBT at RT and before being incubated with secondary antibody in PBTB for 90 min at RT. LHs were then rinsed three times (20 min each) in PBT at RT, before being equilibrated overnight in Citifluor mounting media (Agar Scientific). Discs were then further dissected and mounted. Images were acquired on a Zeiss Apotome2 or Leica Thunder microscope and processed and quantified using Zen, Las X or ImageJ. Primary antibodies used were rabbit anti-cleaved *Drosophila* Dcp-1 (9578, Cell Signaling Technologies, 1:200), rat anti-DE-Cadherin (DCAD2, Developmental Studies Hybridoma Bank, 1:25), rabbit anti-GFP (A6455, Molecular Probes, 1:200) and mouse anti-Mmp1 (3A6B4, DHSB, 1:25). Secondary antibodies used conjugated to Alexa 350, Alexa 488 or Cy3 were from Jackson ImmunoResearch (1:200).

Quantification methods

Genotypes were tested in batches with controls and 10-20 images corresponding to 10-20 different discs were all acquired on the same microscope with the same exposure settings.

Growth was estimated by the size of the GFP-positive area measured as pixel numbers. Mmp1 intensities were ranked as 'high', 'low' or 'null' by an independent observer with genotypes masked and processed in random order. Graphs and statistics (indicated in the legends) were performed using the GraphPad Prism software.

Acknowledgements

We thank G. Alvès, D. Andrew, D. Eberl, P. Léopold, R. Levayer, C. Maurange, A. Teleman, J. Terman, and T. T. Su for sharing flies. We acknowledge the Bloomington Stock Center, the Vienna Stock Center, the DGRC Kyoto Stock Center, the Developmental Studies Hybridoma Bank, the *Drosophila* facility, the MGX sequencing facility (BioCampus Montpellier, CNRS, INSERM, Université de Montpellier) and FlyBase for their support to our research.

Competing interests

The authors declare no competing or financial interests.

Author contributions

Conceptualization: A.D.; Methodology: A.D.; Software: R.L., B.F., J.C.; Validation: R.L., C.G., P.L., M.R.-V., D.K., L.H.-M., B.F., A.D.; Formal analysis: R.L., C.G., P.L., L.H.-M., B.F., J.C., A.D.; Investigation: R.L., C.G., P.L., M.R.-V., D.K., L.H.-M., B.F., A.D.; Data curation: R.L., C.G., P.L., A.D.; Writing - original draft: R.L., S.J.B., A.D.; Writing - review & editing: S.J.B., A.D.; Visualization: R.L., C.G., P.L., J.C., A.D.; Supervision: S.J.B., A.D.; Project administration: A.D.; Funding acquisition: S.J.B., A.D.

Funding

The lab of S.J.B. is supported by the Medical Research Council (MRC programme grant MR/L007177/1). R.L. was supported by fellowships from the Ligue Contre le Cancer and from the Fondation ARC pour la Recherche sur le Cancer. The lab of A.D. is supported by the Fondation ARC pour la Recherche sur le Cancer, a Marie Curie Career Integration Grant (PCIG13-GA-2013-618371) and the Agence Nationale de la Recherche (ANR-18-CE14-0041).

Data availability

RNA-Seq and ChIP data have been deposited in NCBI's Gene Expression Omnibus under accession numbers GSE185339 and GSE185490.

References

Anders, S. and Huber, W. (2010). Differential expression analysis for sequence count data. *Genome Biol.* **11**, R106. doi:10.1186/gb-2010-11-10-r106

Atkins, M., Potier, D., Romanelli, L., Jacobs, J., Mach, J., Hamaratoglu, F., Aerts, S. and Halder, G. (2016). An ectopic network of transcription factors regulated by hippo signaling drives growth and invasion of a malignant tumor model. *Curr. Biol.* **26**, 2101-2113. doi:10.1016/j.cub.2016.06.035

Baeg, G.-H., Zhou, R. and Perrimon, N. (2005). Genome-wide RNAi analysis of JAK/STAT signaling components in Drosophila. *Genes Dev.* **19**, 1861-1870. doi:10.1101/gad.1320705

Banks, L., Pim, D. and Thomas, M. (2012). Human tumour viruses and the deregulation of cell polarity in cancer. *Nat. Rev. Cancer* **12**, 877-886. doi:10.1038/nrc3400

Bilder, D., Schober, M. and Perrimon, N. (2003). Integrated activity of PDZ protein complexes regulates epithelial polarity. *Nat. Cell Biol.* **5**, 53-58. doi:10.1038/ncb897

Bray, S. J. (2016). Notch signalling in context. *Nat. Rev. Mol. Cell Biol.* **17**, 722-735. doi:10.1038/nrm.2016.94

Brumby, A. M. and Richardson, H. E. (2003). scribble mutants cooperate with oncogenic Ras or Notch to cause neoplastic overgrowth in Drosophila. *EMBO J.* **22**, 5769-5779. doi:10.1093/emboj/cdg548

Bunker, B. D., Nellimoottil, T. T., Boileau, R. M., Classen, A. K. and Bilder, D. (2015). The transcriptional response to tumorigenic polarity loss in Drosophila. *eLife* **4**, e03189. doi:10.7554/eLife.03189

Coopman, P. and Djiane, A. (2016). Adherens Junction and E-Cadherin complex regulation by epithelial polarity. *Cell. Mol. Life Sci.* **73**, 3535-3553. doi:10.1007/s00018-016-2260-8

Cordenonsi, M., Zanconato, F., Azzolin, L., Forcato, M., Rosato, A., Frasson, C., Inui, M., Montagner, M., Parenti, A. R., Poletti, A. et al. (2011). The Hippo transducer TAZ confers cancer stem cell-related traits on breast cancer cells. *Cell* **147**, 759-772. doi:10.1016/j.cell.2011.09.048

Cordero, J. B., Macagno, J. P., Stefanatos, R. K., Strathdee, K. E., Cagan, R. L. and Vidal, M. (2010). Oncogenic Ras diverts a host TNF tumor suppressor activity into tumor promoter. *Dev. Cell* **18**, 999-1011. doi:10.1016/j.devcel.2010.05.014

Davie, K., Jacobs, J., Atkins, M., Potier, D., Christiaens, V., Halder, G. and Aerts, S. (2015). Discovery of transcription factors and regulatory regions driving in vivo tumor development by ATAC-seq and FAIRE-seq open chromatin profiling. *PLoS Genet.* **11**, e1004994. doi:10.1371/journal.pgen.1004994

Djiane, A., Krejci, A., Bernard, F., Fexova, S., Millen, K. and Bray, S. J. (2013). Dissecting the mechanisms of Notch induced hyperplasia. *EMBO J.* **32**, 60-71. doi:10.1038/emboj.2012.326

Djiane, A., Zaessinger, S., Babaoğlan, A. B. and Bray, S. J. (2014). Notch inhibits Yorkie activity in Drosophila wing discs. *PLoS ONE* **9**, e106211. doi:10.1371/journal.pone.0106211

Doggett, K., Turkel, N., Willoughby, L. F., Ellul, J., Murray, M. J., Richardson, H. E. and Brumby, A. M. (2015). BTB-zinc finger oncogenes are required for Ras and Notch-driven tumorigenesis in Drosophila. *PLoS ONE* **10**, e0132987. doi:10.1371/journal.pone.0132987

Donohoe, C. D., Csordás, G., Correia, A., Jindra, M., Klein, C., Habermann, B. and Uhlirova, M. (2018). Atf3 links loss of epithelial polarity to defects in cell differentiation and cytoarchitecture. *PLoS Genet.* **14**, e1007241. doi:10.1371/journal.pgen.1007241

Flaherty, M. S., Zavadil, J., Ekas, L. A. and Bach, E. A. (2009). Genome-wide expression profiling in the Drosophila eye reveals unexpected repression of notch signaling by the JAK/STAT pathway. *Dev. Dyn.* **238**, 2235-2253. doi:10.1002/dvdy.21989

Frankenreiter, L., Gahr, B. M., Schmid, H., Zimmermann, M., Deichsel, S., Hoffmeister, P., Turkiewicz, A., Borggrefe, T., Oswald, F. and Nagel, A. C. (2021). Phospho-site mutations in transcription factor suppressor of hairless impact Notch signaling activity during hematopoiesis in Drosophila. *Front. Cell Dev. Biol.* **9**, 658820. doi:10.3389/fcell.2021.658820

Fre, S., Huyghe, M., Mourikis, P., Robine, S., Louvard, D. and Artavanis-Tsakonas, S. (2005). Notch signals control the fate of immature progenitor cells in the intestine. *Nature* **435**, 964-968. doi:10.1038/nature03589

Hamaratoglu, F. and Atkins, M. (2020). Rounding up the usual suspects: assessing Yorkie, AP-1, and Stat coactivation in tumorigenesis. *Int. J. Mol. Sci.* **21**, E4580. doi:10.3390/ijms21134580

Ho, D. M., Pallavi, S. K. and Artavanis-Tsakonas, S. (2015). The Notch-mediated hyperplasia circuitry in Drosophila reveals a Src-JNK signaling axis. *eLife* **4**, e05996. doi:10.7554/eLife.05996

Huang, L. and Muthuswamy, S. K. (2010). Polarity protein alterations in carcinoma: a focus on emerging roles for polarity regulators. *Curr. Opin. Genet. Dev.* **20**, 41-50. doi:10.1016/j.gde.2009.12.001

Igaki, T., Pagliarini, R. A. and Xu, T. (2006). Loss of cell polarity drives tumor growth and invasion through JNK activation in Drosophila. *Curr. Biol.* **16**, 1139-1146. doi:10.1016/j.cub.2006.04.042

Igaki, T., Pastor-Pareja, J. C., Aonuma, H., Miura, M. and Xu, T. (2009). Intrinsic tumor suppression and epithelial maintenance by endocytic activation of Eiger/TNF signaling in Drosophila. *Dev. Cell* **16**, 458-465. doi:10.1016/j.devcel.2009.01.002

Janky, R., Verfaillie, A., Imrichová, H., Van de Sande, B., Standaert, L., Christiaens, V., Hulselmans, G., Herten, K., Naval Sanchez, M., Potier, D. et al. (2014). iRegulon: from a gene list to a gene regulatory network using large motif and track collections. *PLoS Comput. Biol.* **10**, e1003731. doi:10.1371/journal.pcbi.1003731

Katheder, N. S., Khezri, R., O'Farrell, F., Schultz, S. W., Jain, A., Rahman, M. M., Schink, K. O., Theodossiou, T. A., Johansen, T., Juhász, G. et al. (2017). Microenvironmental autophagy promotes tumour growth. *Nature* **541**, 417-420 doi:10.1038/nature20815

Külshammer, E., Mundorf, J., Kilinc, M., Frommolt, P., Wagle, P. and Uhlirova, M. (2015). Interplay among Drosophila transcription factors Ets21c, Fos and Ftz-F1 drives JNK-mediated tumor malignancy. *Dis. Model. Mech.* **8**, 1279-1293. doi:10.1242/dmm.020719

Loubiere, V., Papadopoulos, G. L., Szabo, Q., Martinez, A.-M. and Cavalli, G. (2020). Widespread activation of developmental gene expression characterized by PRC1-dependent chromatin looping. *Sci. Adv.* **6**, eaax4001. doi:10.1126/sciadv.aax4001

Maraver, A., Fernández-Marcos, P. J., Herranz, D., Cañamero, M., Muñoz-Martin, M., Gómez-López, G., Mulero, F., Megías, D., Sanchez-Carbayo, M., Shen, J. et al. (2012). Therapeutic effect of γ-secretase inhibition in KrasG12V-driven non-small cell lung carcinoma by derepression of DUSP1 and inhibition of ERK. *Cancer Cell* **22**, 222-234. doi:10.1016/j.ccr.2012.06.014

McCaffrey, L. M., Montalbano, J. A., Mihai, C. and Macara, I. G. (2012). Loss of the Par3 polarity protein promotes breast tumorigenesis and metastasis. *Cancer Cell* **22**, 601-614. doi:10.1016/j.ccr.2012.10.003

Ntziachristos, P., Lim, J. S., Sage, J. and Aifantis, I. (2014). From fly wings to targeted cancer therapies: a centennial for notch signaling. *Cancer Cell* **25**, 318-334. doi:10.1016/j.ccr.2014.02.018

Ohsawa, S., Sugimura, K., Takino, K., Xu, T., Miyawaki, A. and Igaki, T. (2011). Elimination of oncogenic neighbors by JNK-mediated engulfment in Drosophila. *Dev. Cell* **20**, 315-328. doi:10.1016/j.devcel.2011.02.007

Pagliarini, R. A. and Xu, T. (2003). A genetic screen in Drosophila for metastatic behavior. *Science* **302**, 1227-1231. doi:10.1126/science.1088474

Pascual, J., Jacobs, J., Sansores-Garcia, L., Natarajan, M., Zeitlinger, J., Aerts, S., Halder, G. and Hamaratoglu, F. (2017). Hippo reprograms the transcriptional response to Ras signaling. *Dev. Cell* **42**, 667-680.e4. doi:10.1016/j.devcel.2017.08.013

Ranganathan, P., Weaver, K. L. and Capobianco, A. J. (2011). Notch signalling in solid tumours: a little bit of everything but not all the time. *Nat. Rev. Cancer* **11**, 338-351. doi:10.1038/nrc3035

Reddy, K. L., Rovani, M. K., Wohlwill, A., Katzen, A. and Storti, R. V. (2006). The Drosophila Par domain protein l gene, Pdp1, is a regulator of larval growth, mitosis and endoreplication. *Dev. Biol.* **289**, 100-114. doi:10.1016/j.ydbio.2005.10.042

Reinke, A. W., Baek, J., Ashenberg, O. and Keating, A. E. (2013). Networks of bZIP protein-protein interactions diversified over a billion years of evolution. *Science* **340**, 730-734. doi:10.1126/science.1233465

St Johnston, D. and Ahringer, J. (2010). Cell polarity in eggs and epithelia: parallels and diversity. *Cell* **141**, 757-774. doi:10.1016/j.cell.2010.05.011

Thurmond, J., Goodman, J. L., Strelets, V. B., Attrill, H., Gramates, L. S., Marygold, S. J., Matthews, B. B., Millburn, G., Antonazzo, G., Trovisco, V. et al. (2019). FlyBase 2.0: the next generation. *Nucleic Acids Res.* **47**, D759-D765 doi:10.1093/nar/gky1003

Toedling, J., Skylar, O., Sklyar, O., Krueger, T., Fischer, J. J., Sperling, S. and Huber, W. (2007). Ringo–an R/Bioconductor package for analyzing ChIP-chip readouts. *BMC Bioinformatics* **8**, 221. doi:10.1186/1471-2105-8-221

Toggweiler, J., Willecke, M. and Basler, K. (2016). The transcription factor Ets21C drives tumor growth by cooperating with AP-1. *Sci. Rep.* **6**, 34725. doi:10.1038/srep34725

Turkel, N., Sahota, V. K., Bolden, J. E., Goulding, K. R., Doggett, K., Willoughby, L. F., Blanco, E., Martin-Blanco, E., Corominas, M., Ellul, J. et al. (2013). The BTB-zinc finger transcription factor abrupt acts as an epithelial oncogene in Drosophila melanogaster through maintaining a progenitor-like cell state. *PLoS Genet.* **9**, e1003627. doi:10.1371/journal.pgen.1003627

Uhlirova, M. and Bohmann, D. (2006). JNK- and Fos-regulated Mmp1 expression cooperates with Ras to induce invasive tumors in Drosophila. *EMBO J.* **25**, 5294-5304. doi:10.1038/sj.emboj.7601401

Verfaillie, A., Imrichova, H., Janky, R. and Aerts, S. (2015). iRegulon and i-cisTarget: reconstructing regulatory networks using motif and track enrichment. *Curr. Protoc. Bioinformatics* **52**, 2.16.1-2.16.39. doi:10.1002/0471250953.bi0216s52

Wu, M., Pastor-Pareja, J. C. and Xu, T. (2010). Interaction between Ras(V12) and scribbled clones induces tumour growth and invasion. *Nature* **463**, 545-548. doi:10.1038/nature08702

Xia, S., VanKuren, N. W., Chen, C., Zhang, L., Kemkemer, C., Shao, Y., Jia, H., Lee, U. J., Advani, A. S., Gschwend, A. et al. (2021). Genomic analyses of new genes and their phenotypic effects reveal rapid evolution of essential functions in Drosophila development. *PLoS Genet.* **17**, e1009654. doi:10.1371/journal.pgen.1009654

Xue, B., Krishnamurthy, K., Allred, D. C. and Muthuswamy, S. K. (2013). Loss of Par3 promotes breast cancer metastasis by compromising cell-cell cohesion. *Nat. Cell Biol.* **15**, 189-200. doi:10.1038/ncb2663

SUPPLEMENTARY MATERIALS AND METHODS

Drosophila genetics

Driver lines were *Bx-Gal4* (wing disc pouch), *Dpp-Gal4*, and *Ptc-Gal4* (both wing disc antero-posterior boundary). Overexpression lines were *UAS Nicd* (made by the Bray lab), *UAS GFP:Act87E [7-6]* BL#9249, and *UAS Pdp1.T* BL#78087.

Overexpression lines tested in the *Bx-Gal4, UAS GFP;; UAS Nicd, UAS scribHMS01490* screen were *UAS GFP*, *UAS bskK53R [20.1a]* BL#9311, and *UAS SOD CAT* (gift from P. Leopold). RNAi lines used are listed in the table below with an indication of the labels used in Fig. 4E&F. TRiP collection lines have a stock BL#, and Vienna collection lines have a stock v#. While performing the *Bx>NS* modifier experiments, we used controls originating from the same collection: *RNAi white* for TRiP lines, and *RNAi yellow* for Vienna KK lines.

Gene	RNAi ID	Stock #
Act87E	HMS02488	BL#42642
Act87E	KK111781	v#102480
cdi	KK100725	v#109409
CG7059	GD10763	v#21651
CG13850	KK104804	v#100863
CG13857	GD6226	v#44061
CG18596	KK104660	v#108183
ftz-f1	HMS00019	BL#33625
Ir87a	HMJ22848	BL#60476
Ir87a	KK106593	v#100667
kay	HMS00254	BL#33379
p53	HMS02286	BL#41720
Pdp1	HMS02030	BL#40863
Pdp1	KK109014	v#110551
REG	KK102083	v#110156
stat92E	HMS00035	BL#33637

vito	KK111866		v#102513
w	HMS00045		BL#33644
y	KK104196		v#106068
yellow-e	HMC06250		BL#65970
yellow-e	KK106243		v#100926
yellow-e3	KK106158		v#105879
yki	HMS00041		BL#34067

Primers

qPCR primers:

Act5C_F: Act5C_R: GAGCGCGGTTACTCTTTCAC

Act87E_F: ACTTCTCCAACGAGGAGCTG

Act87E_R: Atf3_F: GTCCACCGCAAGTGCTTCTA

Atf3_R: TTTCTTTGGATGGCAGGGCA

Diap1_F: CAGCATGGCAACATTGGGAC

Diap1_R: ATGAAGGCAGTGGCTGAGTC

E2f1_F: CAGCCACACGCATCTTCAAC

E2f1_R: ACTTTGTCACAGAGGAGGCG

Ets21C_F: ACAGAATCCTCGCCTCCAAC

Ets21C_R: ftz-f1_F: GACTGCTGCCGTAGCCTATT

ftz-f1_R: CTGCTCGCTGATTCGTCCAA

mxc_F: TAGGCATACCGCTTTCCGTG

mxc_R: ATTCCTGGTCGGACATGCTT

p38a_F: TTCATGCAGACATAGTCGCCC

p38a_R: ACTAGAGGAGGAGCAGCGAA

CTAGTGGACAGCGGCGTATT

TACGGACAGGTGTCAAAGGC

CAGCGATCCATTAGCGGGAT

p53_F: TGCGTGTGTTCCTTTGCTTC

p53_R: GTTCAGGGGGACTACAACGG

puc_F: ATTGACCTCGCCGCCAATTA

puc_R: ATTCCGCTTGAACAGAGCCA

sd_F: sd_R: AGGGTCCACAGAATGCGTTT

Sdr_F: TCGCTTTCCACCTTCTCCAC

CGCTCCCTCAATCCCAAAGT

Sdr_R: ACAACGTCCATCAGCCAGTT

Ser_F: GCACGAATCTCTGGTGTGGA

Ser_R: TAGATTTGGCTGGCAGTCGG

wg_F: wg_R: GCAGTCTGGTCTGGTCTACG

Wnt10_F: ATTGTGCGGGTTCAGTTGGA

Wnt10_R: AATGGCATCGGTGGAACTGT

CAGCGTCTTGCGATTGATGG

qChIP primers:

E(spl)mβ_F: AAGTCGGAGCTTTGAATGAG

E(spl)mβ_R: CAAGTCATTTTATTGCCCTCAC

E(spl)m5_F: GTTTCCGCAGGTCCAGTTAC

E(spl)m5_R: GTTTGATGTTCACGCTGCTG

white_F: CGAAGGACGTTGACACATTG

white_R: GAATTGCCGCTTTTTCTCAC

DDC_F: AAGTGGGATTTGCCAGTGAC

DDC_R: TGCTGGTGAACTTTGACTGC

CG42808_F: CTCGTTAAGAGCAACTGCGA

CG42808_R: GTGAGAACTCCGAATCGAGG

CG6191_F: CGAAAAATGCGGACGATTCC

CG6191_R: CCCACCAATCTAGGGTTTCA Ilp8_F:

TCATCTCCGGTGTCTGACTT Ilp8_R:

AAAGAATTGGCTGCGGAAGA

Logeay et al. Figure S1

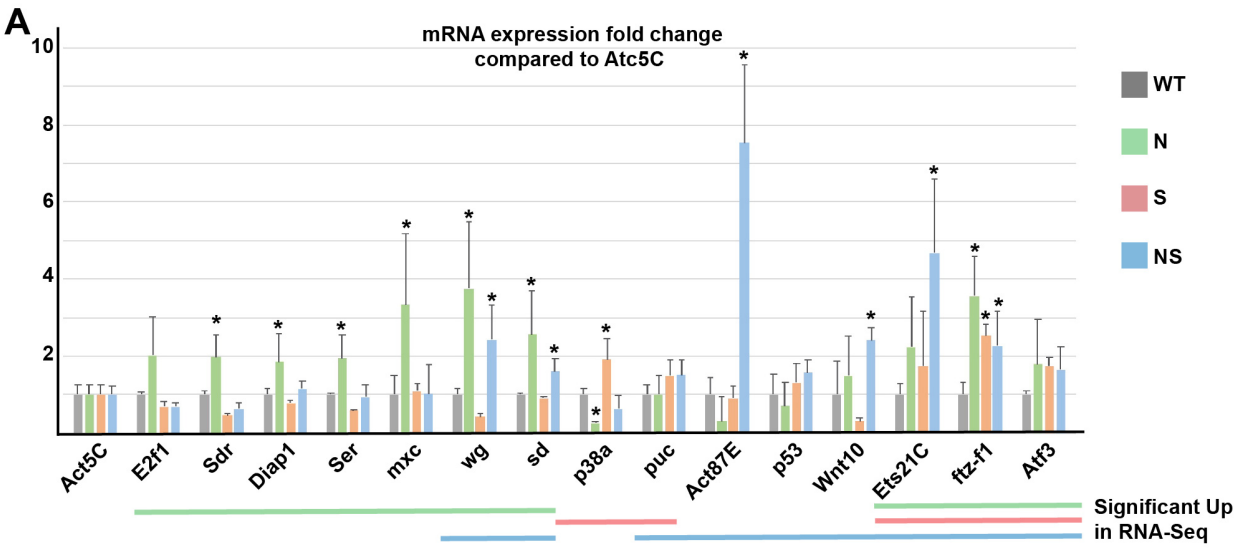

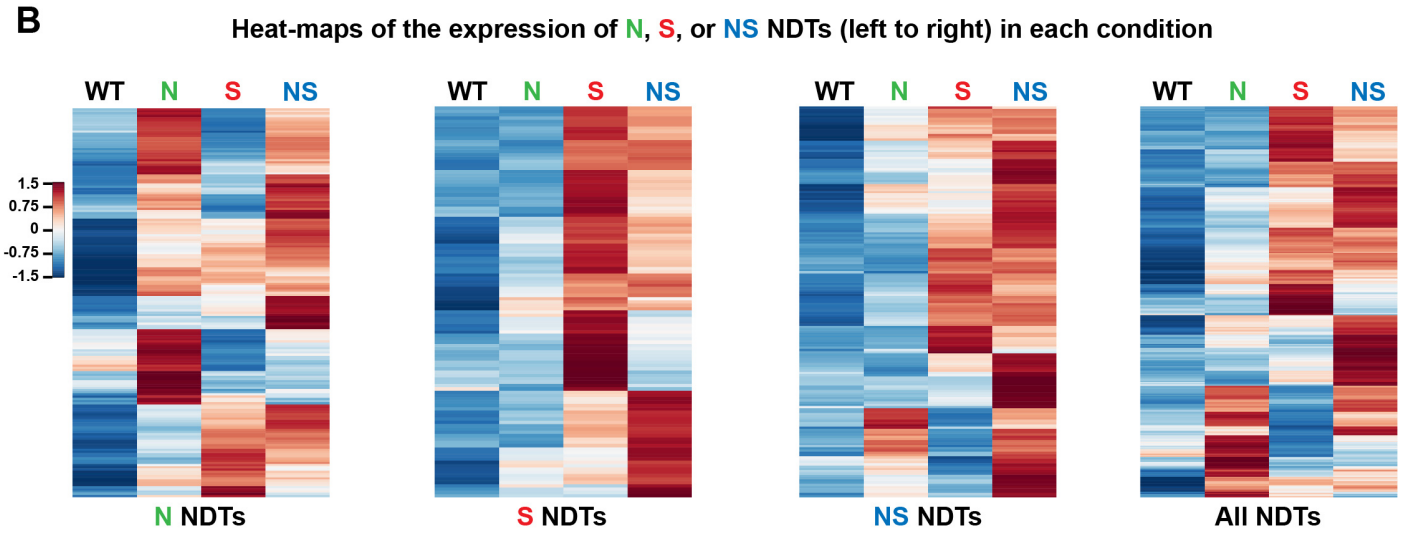

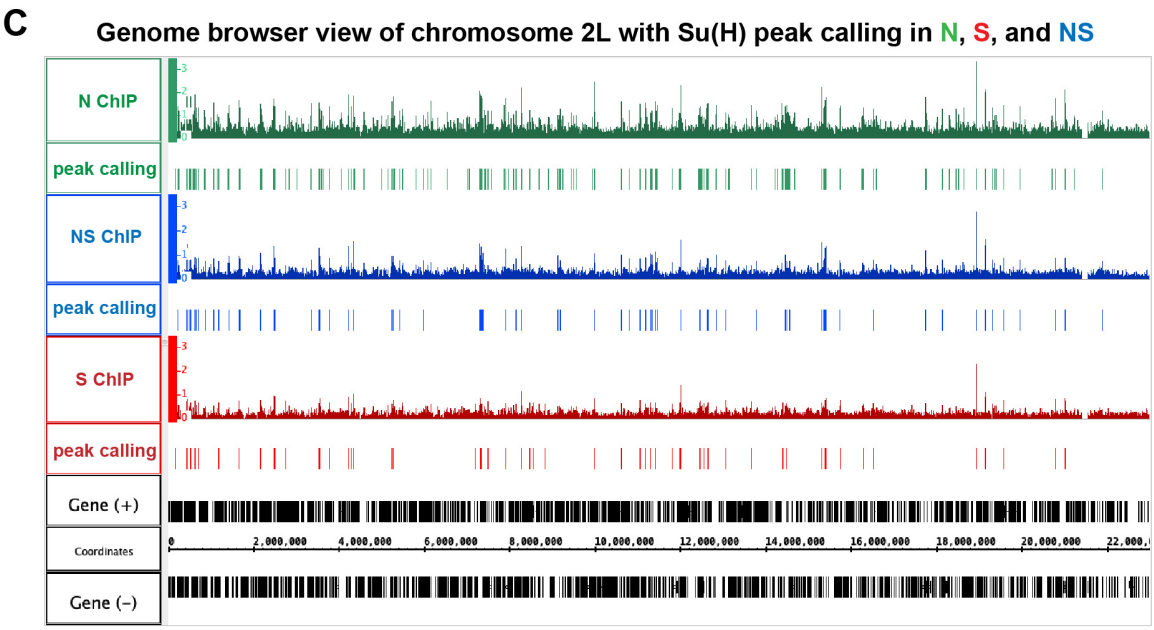

Fig. S1. Features of the Notch Direct Targets (NDTs) in N, S, and NS (relates to Fig. 3)

A. Semi-quantitative RT-PCR of the indicated genes represented as fold change compared to WT (grey) in the different N (green), S (red), and NS (blue) growth paradigms and normalized to *Atc5C* expression. Biological triplicates, standard error to the mean (s.e.m.) is shown. ANOVA statistical test, * $p<0.05$.

B. Heatmaps for the expression of the different NDTs in WT, N, S, and NS. From left to right are presented the N, S, NS, and finally All NDTs, highlighting that NDTs could be transcriptionally up-regulated in more than in one condition.

C. Genome browser view of the whole left arm of the 2nd chromosome, and showing the Su(H) ChIP enrichment (upper rows) and the intervals called as Su(H) peaks (lower rows) in N (green), NS (blue), and S (red). Note the higher number of peaks in N, and the rarity of NS, or S peaks not found in N.

Logeay et al. Figure S2

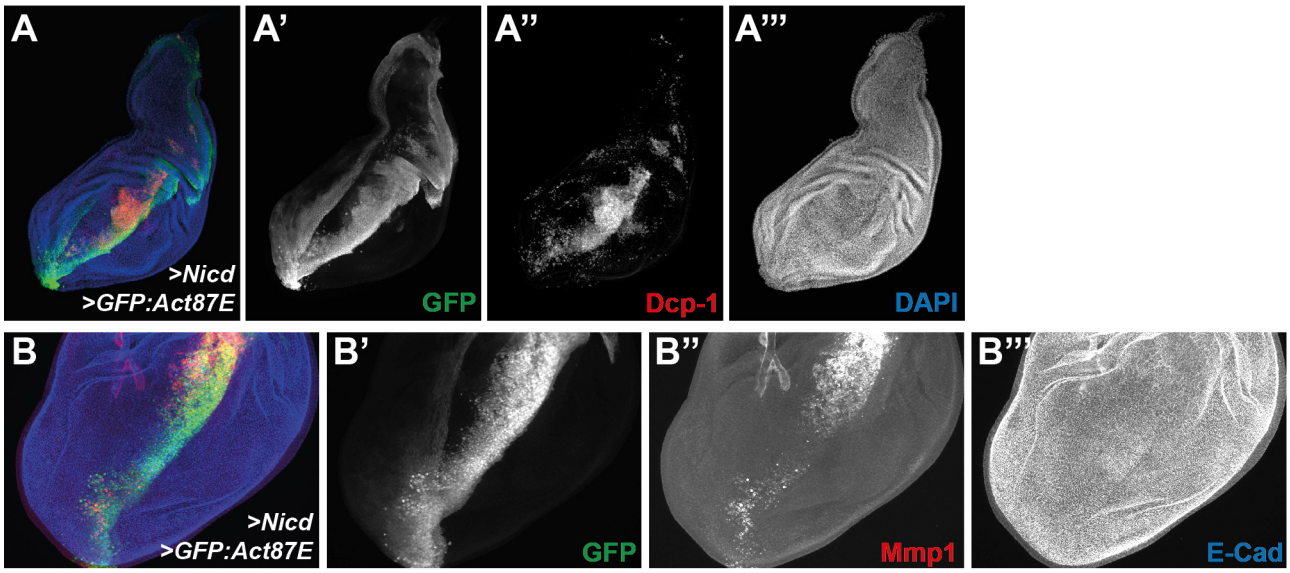

Fig. S2. Act87E promotes Mmp1 expression and cell delamination.

A-B. GFP:Act87E overexpressed together with activated Notch (Nicd) under the control of the *Ptc-Gal4* driver (antero/posterior boundary cells in green, A'&B'), promotes the expression of the Dcp-1 caspase (red, A''), and the metalloprotease Mmp1 (red, B''). Similar results were obtained for the sole overexpression of GFP:Act87E (without Nicd). DAPI (blue, A''') or E-Cad (blue, B''') mark all wing disc cells. (A) Whole wing disc. (B) Detail of the overgrowing wing pouch (magnification in B is twice that in A).

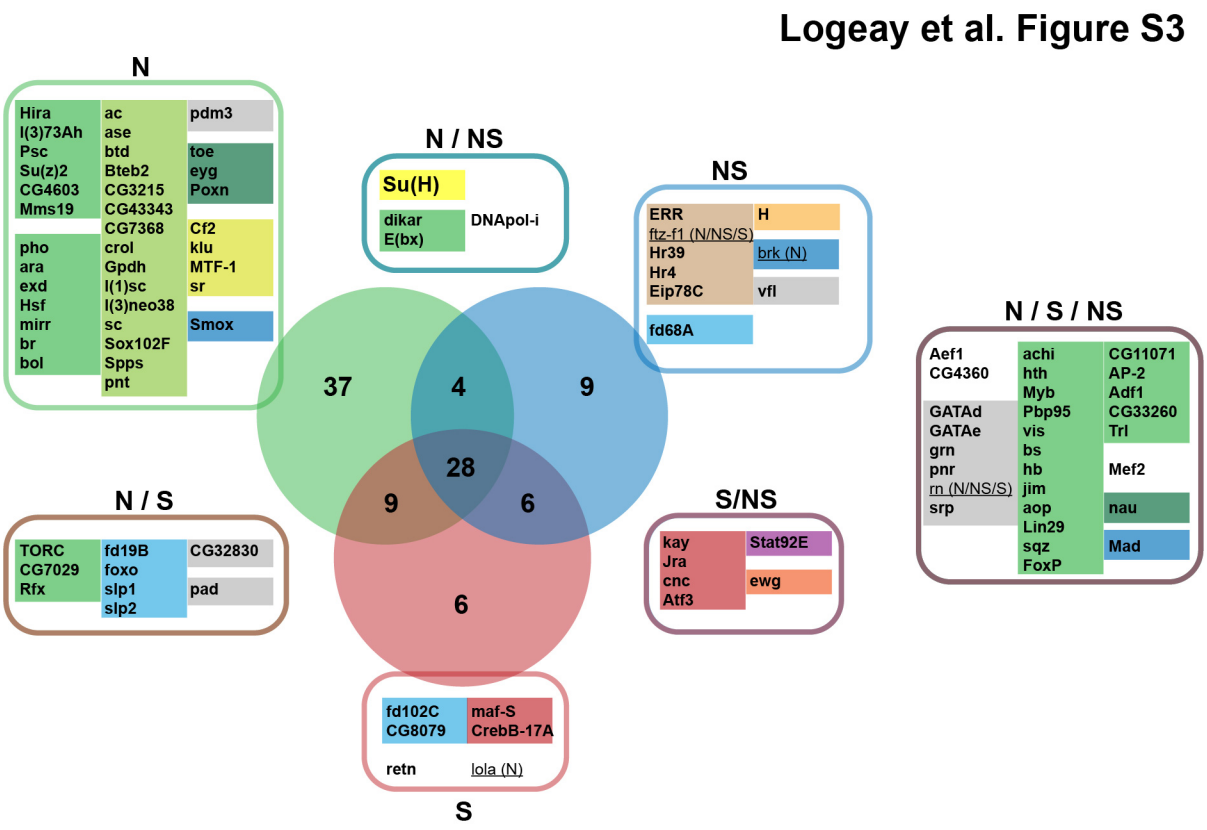

Fig. S3. Identification of potential transcriptional modules mediating N, S, and NS growth (relates to Fig. 3)

Venn diagram of significant transcription factors (TFs) identified by iRegulon as potential key mediators for the expression of the N (in the green circle), S (red circle), and NS (blue circle) Notch Direct Target (NDT) genes. Fed with lists of co-regulated

genes, and analyzing the genomic features in the vicinity of the transcription start sites of these genes, iRegulon identifies potential groups of TFs and DNA-binding factors, that are enriched in the dataset of regulatory sequences, and could thus represent potential mediators regulating the expression of NDT genes in N, S, and NS.

For each condition, TFs were identified as part of "regulons" or group of TFs that could potentially together regulate the expression of subsets of the transcriptome. Taking only the TFs corresponding to the significant regulons identified in N, S, and NS, the shared and unique potentially regulating TFs are here presented in the different colored boxes.

In each box, TFs were then grouped according to their molecular family (suggesting pretty similar binding motifs on the DNA), and color-coded: for instance, bZIP TFs in light maroon, or the nuclear receptors in brown. The molecular family color code was not respected for the green groups which correspond to very diverse "regulons" that appear linked to epigenetic chromatin regulators/remodelers. For the complete list of regulons identified in each condition, and the nature of TFs and DNA binding proteins in each regulon, see Supplemental table S5). Numbers in the Venn diagram represent the number of TFs identified. TFs that are also NDTs and which could participate in feedforward loops are underlined (with their NDT condition in parentheses).

Logeay et al. Figure S4

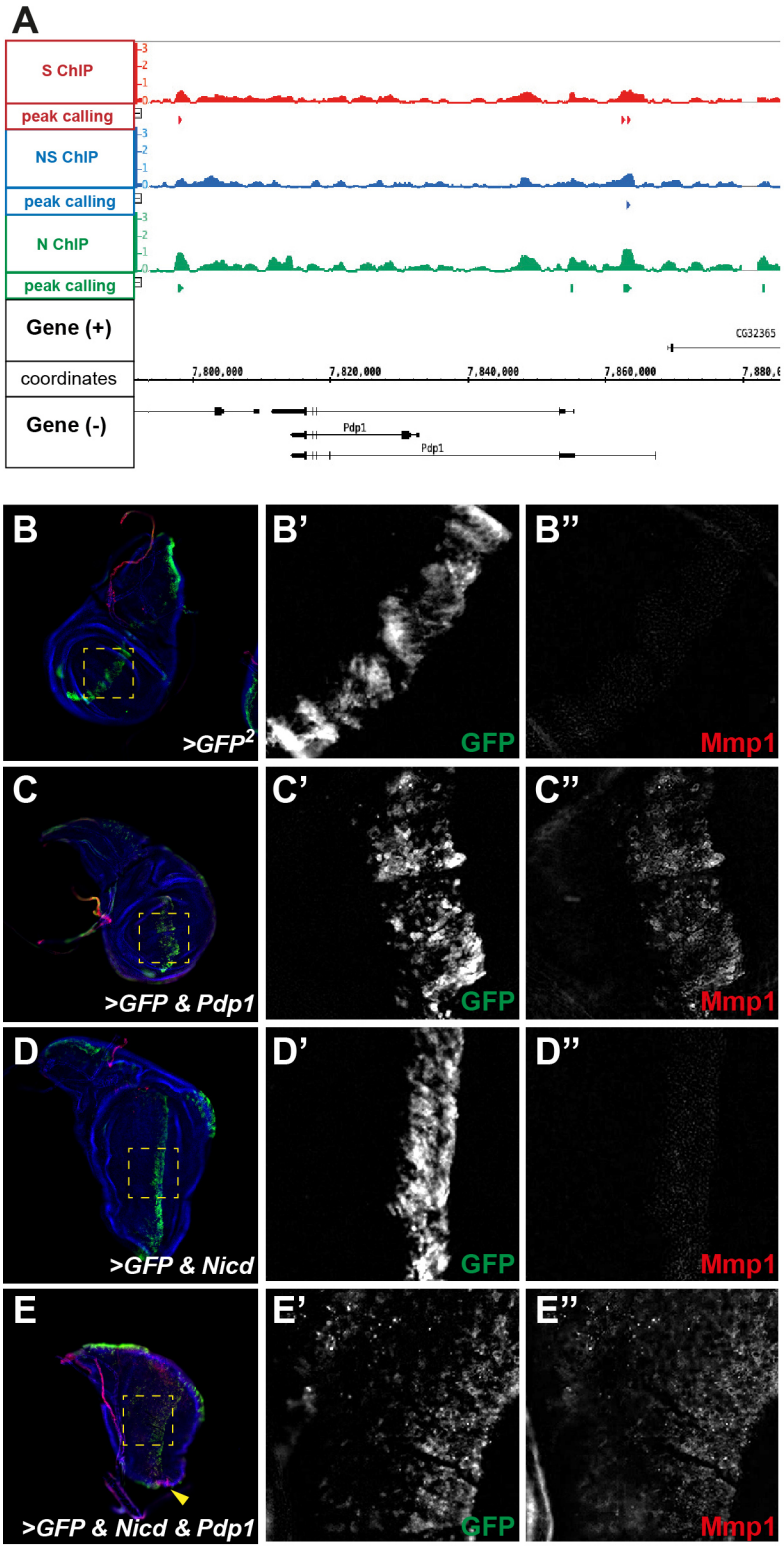

Fig. S4. Pdp1 is a direct Notch target (relates to Fig. 4)

A. Genome browser view of the *Pdp1* locus, and showing the Su(H) ChIP enrichment (upper rows) and the intervals called as Su(H) peaks (lower rows) in N (green), NS (blue), and S (red).

B-E. Pdp1 overexpression causes Mmp1 expression. GFP alone (B) or in combination with *Pdp1* (C), with *Nicd* (D), or with *Nicd & Pdp1* (E) was overexpressed using the *Dpp-Gal4* driver. Higher magnification corresponding to the yellow dashed boxes show GFP in green (B'-E') and Mmp1 in red (B''-E''). E-Cad used as landmark is shown in blue (B-E). Pdp1 overexpression resulted in Mmp1 positive cells extending anteriorly (C). This was enhanced when combined with Nicd (E). Representative discs shown (out of 18 imaged discs from 3 experiments).

(E) Mmp1 expression is found in the *Pdp1&Nicd* overexpressing cells (GFP positive under the influence of the *Dpp-Gal4* driver), but also in non-expressing cells (non- autonomous, yellow arrowhead).

Table S1. Differentially expressed genes in N, S, and NS identified by DESeq (related to Fig. 1).

Columns are:

FBgn_ID: Unique FlyBase gene ID

Symbol: Current FlyBase gene symbol

qval: adjusted p-value for multiple testing

logFC: log2 of the Fold Change “Condition N, S, or NS” / “Control WT”

Click here to download Table S1

Table S2. Su(H) ChIP enrichment peaks coordinates in N, S, and NS (related to Fig. 3).

Columns are:

Exp: N, S, or NS

Chr: Chromosome arm

MIN: smallest peak coordinate

MAX: biggest peak coordinate

Click here to download Table S2

Table S3. All Notch Direct Targets (NDTs) ordered by genomic position. This table includes an indication whether the genes are transcriptionally upregulated or have a Su(H) peak in the vicinity in each N, S, and NS condition. Columns are:

N/NS/S: NDT in the corresponding condition

Type: NDT in different conditions.

FBgn_ID: Unique FlyBase gene ID

SYMBOL: Current FlyBase gene symbol

K_ARM: Chromosome arm location of the gene

MIN (gene pos): smallest gene coordinate

MAX (gene pos): biggest gene coordinate

STRAND: +1 or -1

N Fold: Log2 Fold Change in gene expression N/WT (n.s. not significant)

N ChIP: Su(H) ChIP enrichment peak within 20kb in N (green yes, red no)

NS Fold: Log2 Fold Change in gene expression NS/WT (n.s. not significant)

NS ChIP: Su(H) ChIP enrichment peak within 20kb in NS (green yes, red no)

S Fold: Log2 Fold Change in gene expression S/WT (n.s. not significant)

S ChIP: Su(H) ChIP enrichment peak within 20kb in S (green yes, red no)

Click here to download Table S3

Table S4. Curated iRegulon analyses of the significantly upregulated genes in N, S, and NS (related to Fig. 3). Analyses were performed using the 6K-PWM and 10kb upstream and downstream set-ups.

Click here to download Table S4

Table S5. Curated iRegulon analyses of the Notch Direct Targets in N, S, and NS (related to Fig. S2). Analyses were performed using the 6K-PWM and 10kb upstream and downstream set-ups.

Click here to download Table S5